# 2025年臺灣國際科學展覽會 優勝作品專輯

作品編號 160012

參展科別 物理與天文學

作品名稱 Wetting Tracing Paper—Fiber Porous

Media Curling Behavior and Mechanisms

就讀學校 高雄市立高雄高級中學

指導教師 盧政良

作者姓名 林永章

關鍵詞 <u>Diffusion、Richard's EquaBon、Finite</u>

<u>Difference Method</u>

## 作者簡介



I am a twelfth-grade student from Kaohsiung Municipal Kaohsiung Senior High School, and I'm thrilled to present my research on the curling and uncurling behavior of tracing paper when exposed to water. This study combines theoretical analysis and hands-on experiments, revealing that while Fick's diffusion model effectively explains the uncurling phase under steady water content, it underestimates the dynamic changes in diffusivity during the initial curling stage. To address this, I applied Richards' equation to capture capillary action within the paper's porous structure, incorporating a finite difference approximation with Robin boundary conditions. By validating experimental data, I discovered key factors affecting curling behavior, including paper thickness, temperature, and salt concentration. I am deeply grateful to my teacher, Mr. Lu-Cheng Liang, for his unwavering guidance, and to my discussion partner, Jun-Yi Lin from Taipei Municipal Chien Kuo High School. I hope to inspire others to explore everyday phenomena through the lens of science.

i

## 2025 年台灣國際科學展覽會

## 研究報告

區別:

科別:物理與天文學科

作品名稱: Wetting Tracing Paper—Fiber Porous Media

**Curling Behavior and Mechanisms** 

關鍵詞: Diffusion、Richard's Equation、Finite Difference

Method

編號:

### **Abstract**

This research presents a novel approach to understanding the curling and uncurling behavior of tracing paper when exposed to water, identifying limitations in traditional diffusion-based models like Fick's second law. While Fick's model adequately represents the uncurling phase, where water content is stable, it falls short during the curling phase due to its inability to account for dynamic changes in diffusivity. Our study identifies capillary action, modeled through Richards' equation, as the primary mechanism in the curling phase, where diffusivity varies with water content due to capillary-driven water movement through the paper's porous structure. Experimental data align well with the Richards' equation model, highlighting a saturation point where curvature peaks, governed by evaporation's impact on moisture balance.

To simulate this phenomenon, we developed a finite difference approximation scheme based on Richards' equation, discretizing the spatial domain for detailed control over moisture dynamics and incorporating the Robin boundary condition with virtual points. This approach, combined with evaporation considerations, produces simulation results consistent with observed data, emphasizing evaporation's role in steady-state moisture gradients and the subsequent deformation mechanics.

Our findings further reveal that factors like paper thickness, temperature, and salt concentration significantly influence curling behavior. We established linear correlations between peak time and thickness reciprocal, as well as between peak curvature and thickness squared, supporting theoretical models. Temperature affects both peak curvature and curling rate due to changes in viscosity and surface tension, and higher temperatures prevent full uncurling due to sustained evaporation effects. Increased salt concentration heightens peak curvature without altering expansion ratio, suggesting additional variables in play.

這項研究指出傳統基於擴散模型的局限性。雖然費克模型能充分描述水分含量穩定的展開階段,但在卷曲階段表現不足,因為它無法考慮擴散率的動態變化。我們的研究確定了通過 Richards 方程式建模的毛細作用作為卷曲階段的主要機制,在該階段,由於毛細驅動的水分通過紙張多孔結構的運動,擴散率隨水分含量而變化。實驗數據與 Richards 方程模型高度吻合,突顯了一個飽和點,此時曲率達到峰值,這由蒸發對濕度平衡的影響所決定。為了模擬這一現象,我們開發了一種基於 Richards 方程的有限差分近似方案,對空間域進行離散化,以詳細控制濕度動態,並結合虛擬點的 Robin 邊界條件。這種方法結合蒸發考量,產生的模擬結果與觀察數據一致,強調了蒸發在穩態濕度梯度及隨後變形機

理中的作用。我們的研究進一步發現,紙張厚度、溫度和鹽濃度等因素顯著影響 卷曲行為。

## Contents

I. Introduction	2
II. Research Methodology	4
(I.)Experimental Setup	4
(II.Cylinders Formation	5
(III.) Curling Direction-Fiber Orientation	6
(IV.) Pore and Fiber Sorption Aspect-Droplet Experiment)	10
III. Qualitative and Quantitative	14
(I.)Mechanism Explanation	14
Diffusion Model Discussion	14
Capillary Model Discussion	14
Richard's Derivation	16
Mere Limiting Case-Diffusive Mathematical Formula	17
(II.) Finite Difference Method - Richards Simulation	19
(IV.)Parameters Discussion	26
(V.)Temperature and Evaporation	27
(VI.)Discussion-Salt Concentration	34
V. Conclusion	36
VI.References	41
Appendix 1: Simulation Code	42
Appendix 2: Finite Difference Approximation for Fick's Second Law	43

## I. Introduction

#### Motivation and Research Purpose

When a tracing paper is gently placed on the surface of water, it rapidly curls into a scroll and then slowly uncurls. This phenomenon is significant as it provides insights into the wetting mechanism of fiber porous materials, particularly tracing paper. This investigation is crucial for designing bio-inspired systems, such as adaptive grippers that mimic natural movements, and for developing soft materials with, moisture-responsive behaviors ideal for applications in soft robotics. Tracing paper, like other fibrous materials, is mainly made of cellulose fibers and has a porous structure. The wetting mechanism in such materials typically involves two key processes: pore sorption and fiber sorption. However in previous studies, tracing paper is hydrophobic, so fiber sorption is not the main process here. Moreover, due to its low porosity, the pore sorption mechanism becomes the dominant factor.

In our literature review, we referenced two key studies on the curling behavior of tracing paper. The first study by [7] used the Washburn equation and molecular diffusion models, but both showed deviations on mechanisms and both partially fitted data. Despite these limitations, the study provided valuable insight, particularly in showing that Fick's law applies during the uncurling phase, assuming constant diffusivity. The second study [6] used Richard's Equation to model capillary action, fully fitting the data for both curling and uncurling phases, as assuming diffusivity changes according to water content. However. In our case, this doesn't exist and only fitted the curling phase. Thus in this investigation, we aim to understand the complete mechanism and to better explain quantitative and qualitative. Thus, moreover we prospect to explain the deviations of the paper.

## Two Referenced Paper Discussed the Phenomenon ⇒ Problems ⇒ Clarify the Mechanism of Wetting Induce Curling

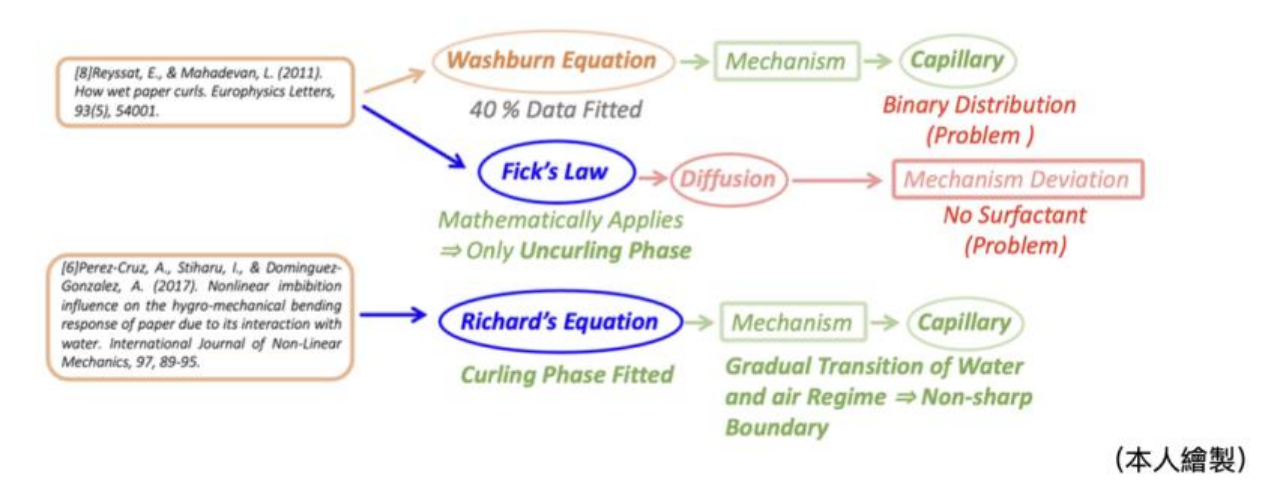


Figure 1: Comparative Analysis of Models Describing Wetting-Induced Curling in Tracing Paper

The schematic presents a comparative analysis of models describing the wetting-induced curling behavior of tracing paper, underscoring specific limitations that call for a more integrated approach. Previous studies have utilized the Washburn equation, Fick's law, and Richards' equation to model different phases of this phenomenon, each with varying levels of applicability.

From the first paper, the Washburn equation, which describes capillary-driven fluid movement, aligns with approximately 40% of our data, capturing an intermediate phase where the curvature approaches its peak and transitions to the uncurling phase. Although it partially describes this transition, its assumptions, such as binary distribution, introduce deviations, limiting its relevance to the complete curling and uncurling dynamics.

Fick's law, although limited in explaining the initial curling mechanism due to its incorrect diffusion-based assumptions, effectively models the uncurling phase. This observation is mathematically valid, as Fick's law applies to diffusion dynamics in the uncurling process. Initially, the presence of surfactants suggested that Fick's law might govern the uncurling mechanism, as substituting water with soapy water showed no change in curvature. However, since surfactant molecules cannot penetrate cellulose surfaces in aqueous solutions (Penfold et al., 2007), they do not affect the water entering the paper. Thus, capillary effects remain significant and should not be disregarded. Fick's law is applied to the uncurling phase, effectively modeling diffusion dynamics under the assumption of constant diffusivity.

In the second paper, Richards' equation is shown to comprehensively fit the entire curling process, effectively modeling a gradual water-air transition and capturing the non-sharp boundary observed. However, our experiments reveal that changing temperature impacts the final curvature, indicating that the system eventually reaches a steady state with saturated diffusivity, leading to a stable peak curvature. At this steady state, Richards' equation essentially becomes a special case of Fick's law with constant, saturated diffusivity. Thus, Richards' equation is best suited to model the curling phase but requires consideration of a saturated diffusivity for full accuracy in describing the transition into a steady state.

By addressing these mechanistic gaps, our study aims to provide a more comprehensive understanding of wetting-induced curling in fibrous materials.

#### Research Framework

This research paper focuses on two insights. First, we clarify the mechanism of wettinginduced curling behavior in tracing paper both qualitatively and quantitatively, providing our own explanations. Second, we discuss the dependencies of various relevant parameters, offering key insights based on our findings. Specifically, we explore the linear relationship between thickness and two crucial parameters—"Peak Time" and "Peak Curvature." For temperature dependence, we clarify deviations in the pore distribution fitting results, contradicted to cylindrical pores approximation, and address the observed linear relationship between maximum diffusivity and saturated diffusivity to the surface tension-viscosity ratio as temperature increases. Additionally, we discuss how temperature influences peak curvature, curling speed, and final curvature, highlighting the evaporation factor in the latter. Finally, we examine the impact of salt concentration on diffusivity and surface tension-viscosity ratio, identifying a linear relationship between these factors. We also find that increasing salt concentration leads to a rise in peak curvature under constant thickness, while the expansion ratio remains unchanged. Since peak curvature is theoretically related only to these two parameters, this observation suggests that other factors might influence peak curvature, warranting further investigation.

## II. Research Methodology

## (I.) Experimental Setup

(本人拍攝)

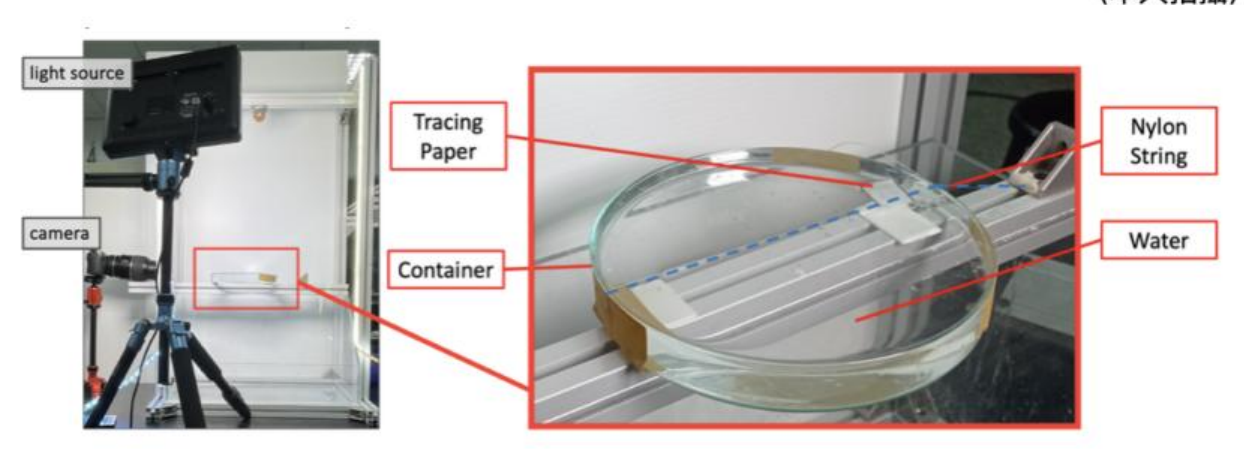
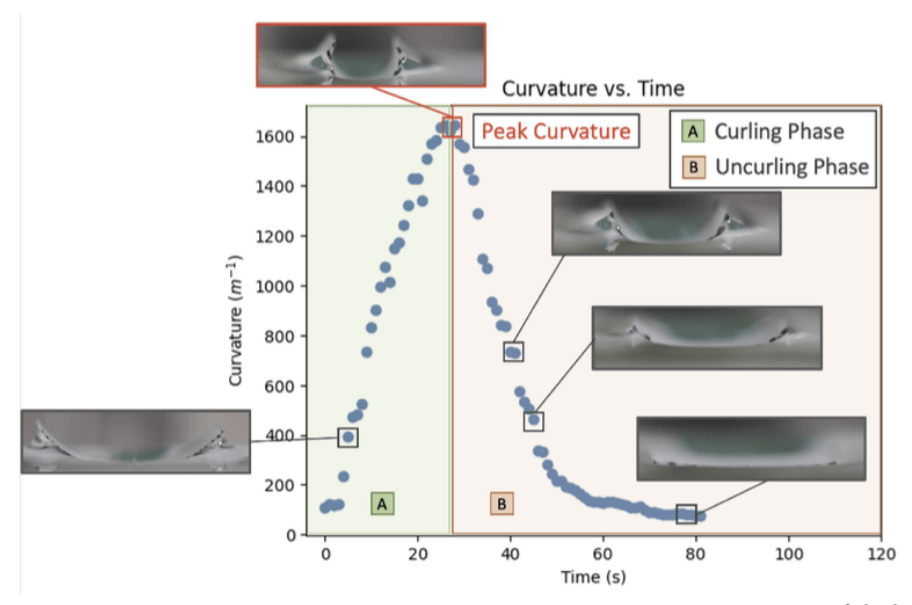


Figure 2: Here we use a container to hold the water. We suspend a nylon string directly on the surface of water to pin the tracing paper in place. When putting tracing paper, we lift the nylon string above the water and use tweezers to place the tracing paper under the string.

#### **Preliminary Observation:**

When the tracing paper was placed on the water's surface, it was observed that the paper initially curled into a cylindrical shape before gradually and slowly uncurling. To better understand this phenomenon, the curvature of the tracing paper was analyzed over time.



(本人分析輸出擷取)

The curvature of tracing paper interacting with water was analyzed using a slow-motion camera positioned parallel to the cylindrical shapes formed during curling. Gaussian curvature ( $\mathcal{K} = \kappa_1 \cdot \kappa_2$ ) was used to describe the surface's curvature, where  $\kappa_1$  and  $\kappa_2$  are the principal curvatures. As the paper curled into a cylindrical shape, it exhibited Zero Gauss Curvature because one curvature was non-zero ( $\kappa_1 \neq 0$ ), while the perpendicular curvature was zero ( $\kappa_2 = 0$ ). This results in a developable surface, characteristic of cylindrical shapes

## (II.)Cylinders Formation

Depending on different initial conditions, the geometry the tracing paper will produce vary. If the CD length is less than the circumference produced by the peak curvature reached, then the two ends of tracing paper will not touch, which we call the 0-scroll. This case is the main phenomenon of study, since it is minimally affected by factors such as friction. If the CD length is bigger than the threshold, then it will curl into a cylindrical shape, dubbed 1-scroll. Whether it sinks at the peak curvature or not depends on whether the gravity exceeds surface surface tension, and they are in turn related to the ratio of MD and CD length and the peak curvature. If the paper is not released perfectly flat, then the two ends will curl at a different time and amount, thus one end will curl and touch the water, producing a scroll in opposite direction, and finally sink and uncurl underwater. If

the paper is released flat enough such that the two ends collide and force each other into cylinders, it will form two cylinders, which we call the 2-scroll.

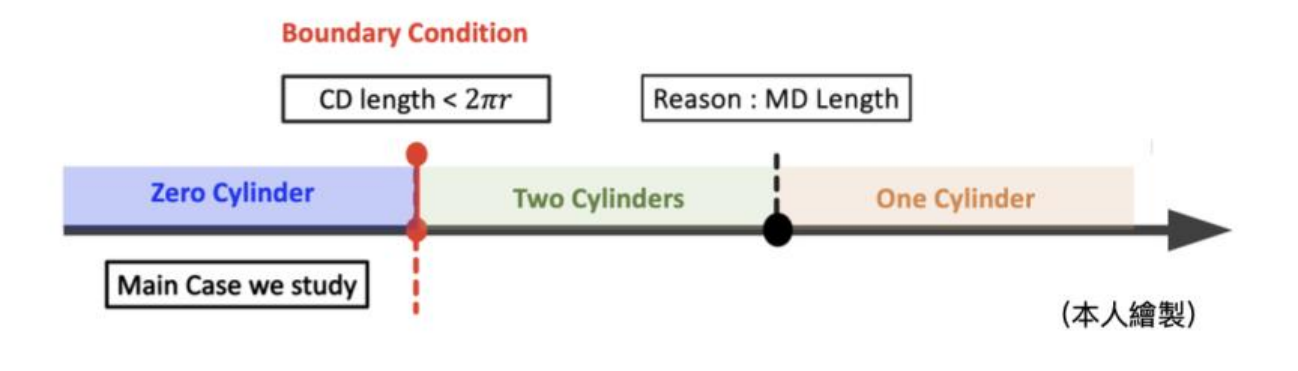




Figure 3: Cylinder Formaiton (本人拍攝)



Figure 4: Failure case (本人拍攝)

### (III.) Curling Direction-Fiber Orientation

In order to use a string to put the paper in place, we shall first predict in what axis the paper will curl; otherwise, the string may affect its curling motion. We define the curling direction as the axis of the cylinder formed by the tracing paper. It is seen by cutting the piece of paper at different angles that the axis of scrolling is always parallel to one of the original edges. (observation, Side A,B C will describe in Figure Two) By observing

the expansion of a piece of fully wet paper, we see that it displays an apparent anisotropy in two perpendicular directions parallel to its original edges. The direction with higher expansion corresponds to the Cross Direction (CD), which is perpendicular to the fiber orientation direction, Machine Direction (MD) **DeRuvo1973**.) These terms originate from the manufacture of paper. As intuition would suggest, the height of the cylindrical shape produced by scrolling is perpendicular to CD, indicating that the direction with higher expansion dominates the scrolling.

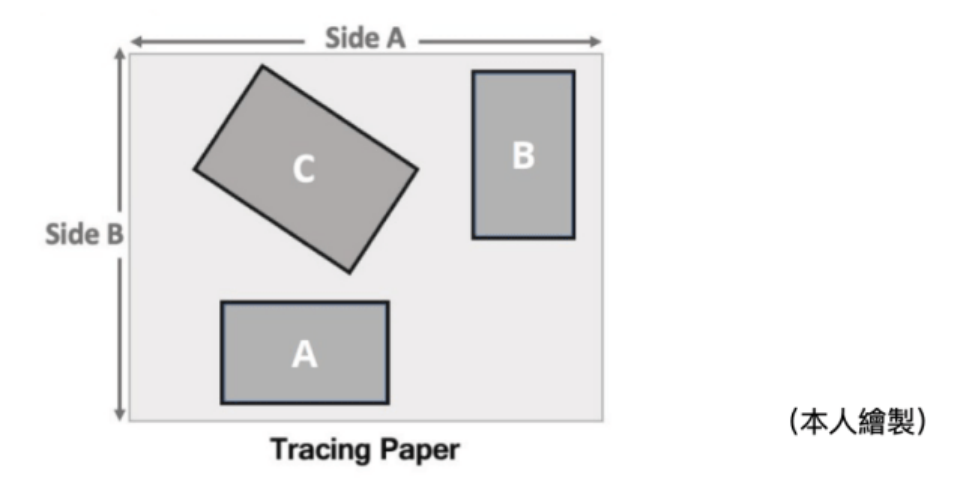
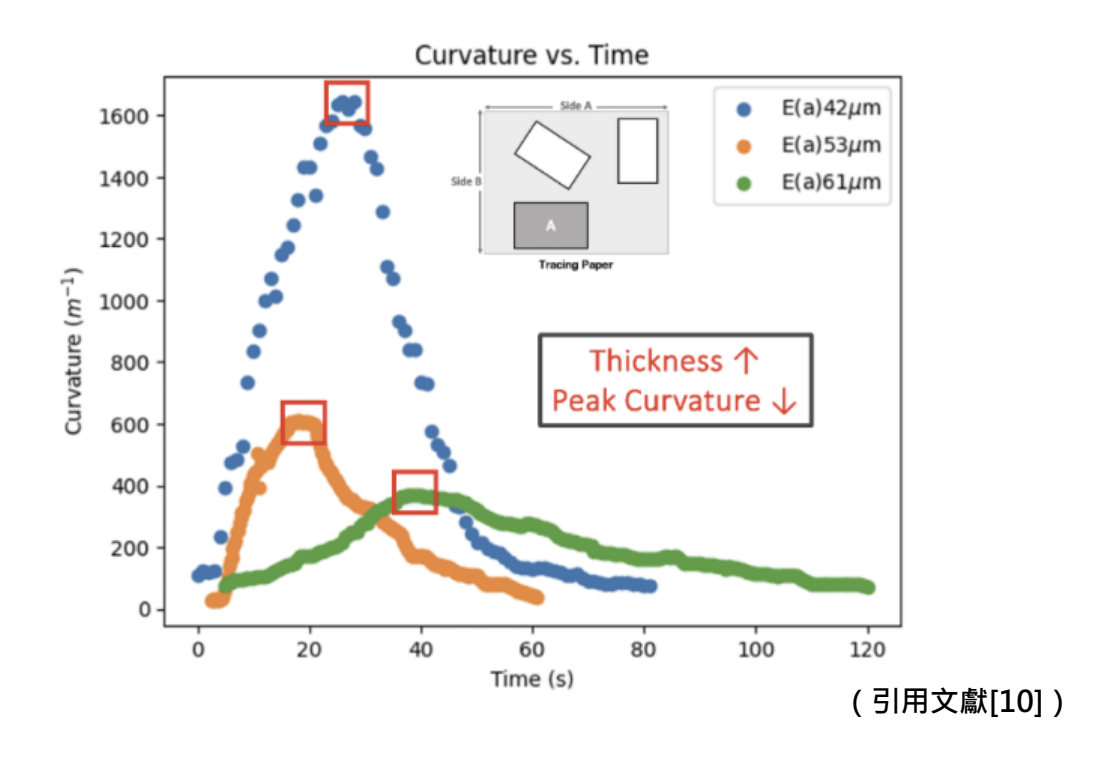
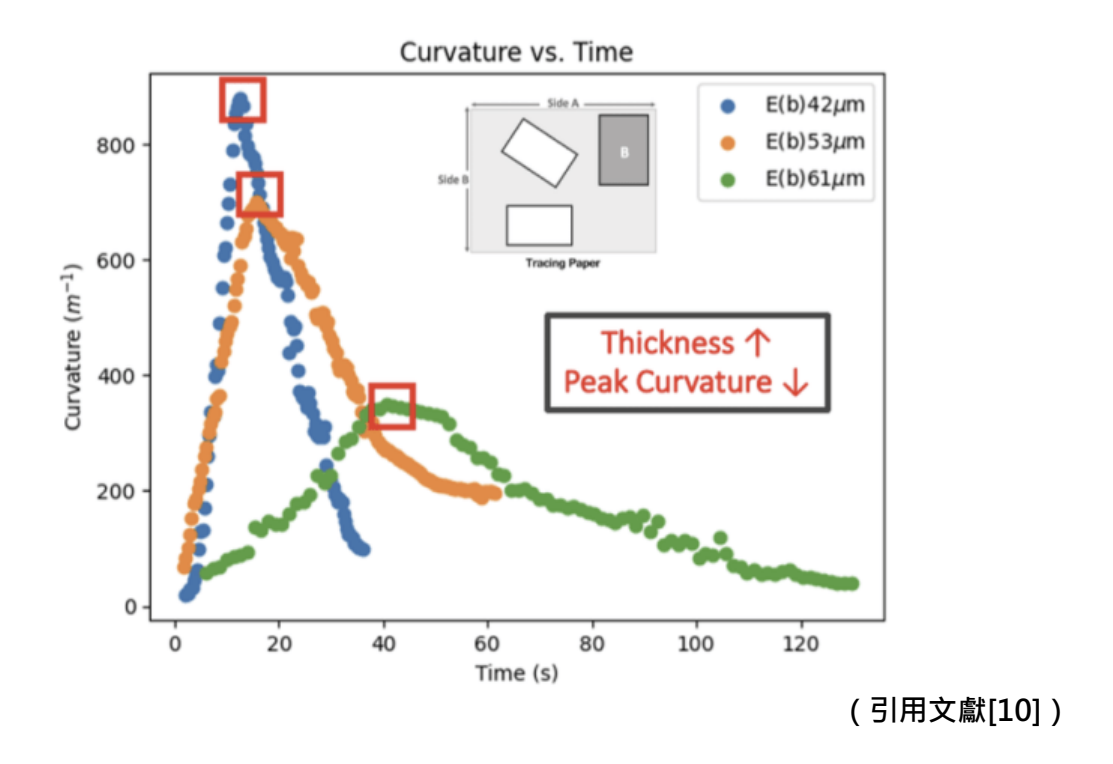


Figure 5: Cut an unaltered piece of paper direct from manufacture in different angles. Their axis of curling are all the same, parallel to the Side B. In this case, Side A corresponds to CD, Side B is MD





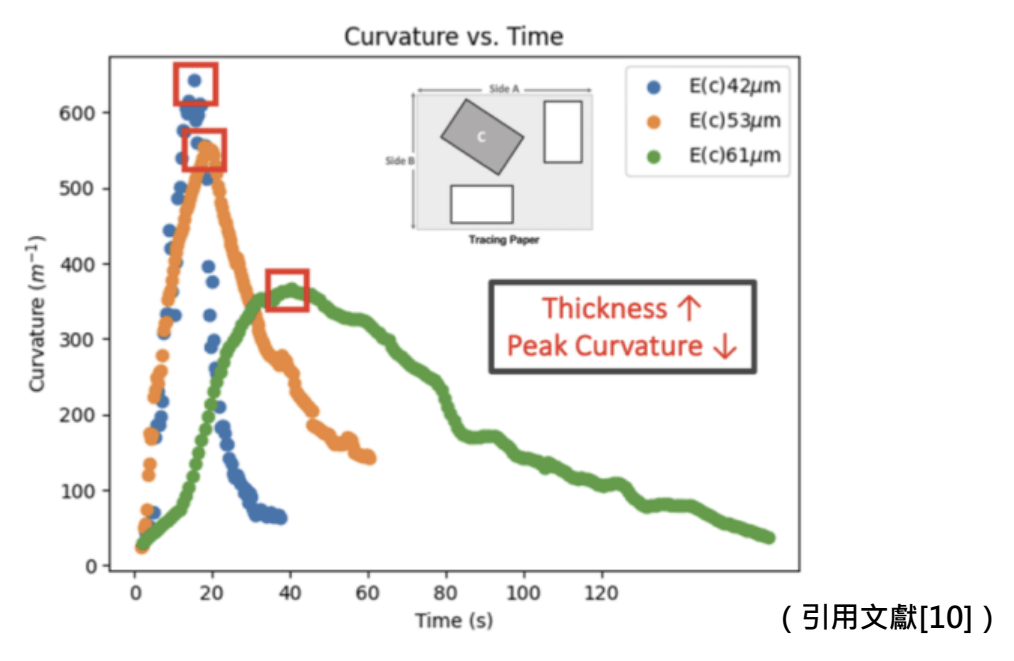


Figure 6: The three graphs are that we tracking curvature of tracing paper in A,B,C directions under different thickness which in Fig.6 mentioned. From the experimental result of curvature to time we can found out two key insights. Firstly, from the three graph we all can found out that when thickness increases peak curvature decreases, peak time increases, which will be qualitatively explained in **parameters discussion** further. Secondly, from the three graphs we can also find that curvature with same thickness in different angle(A,B,C) is different, since tracing paper have been cut in different angle, the MD/CD length differs.

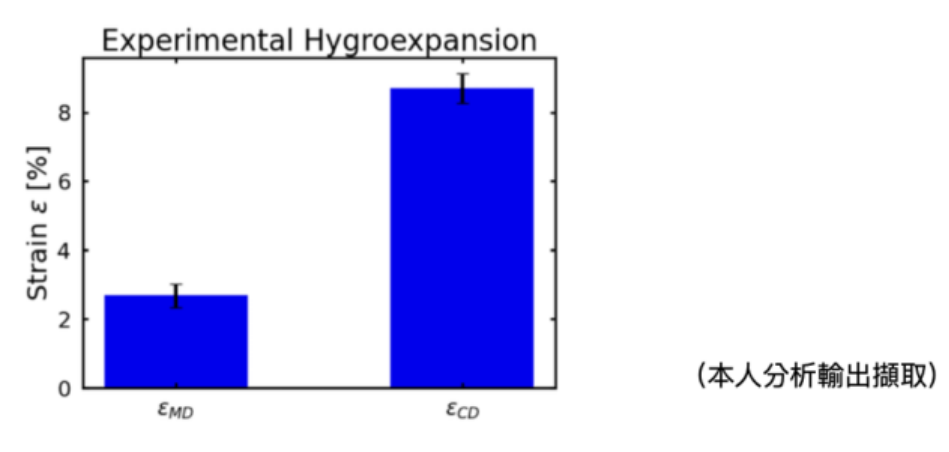


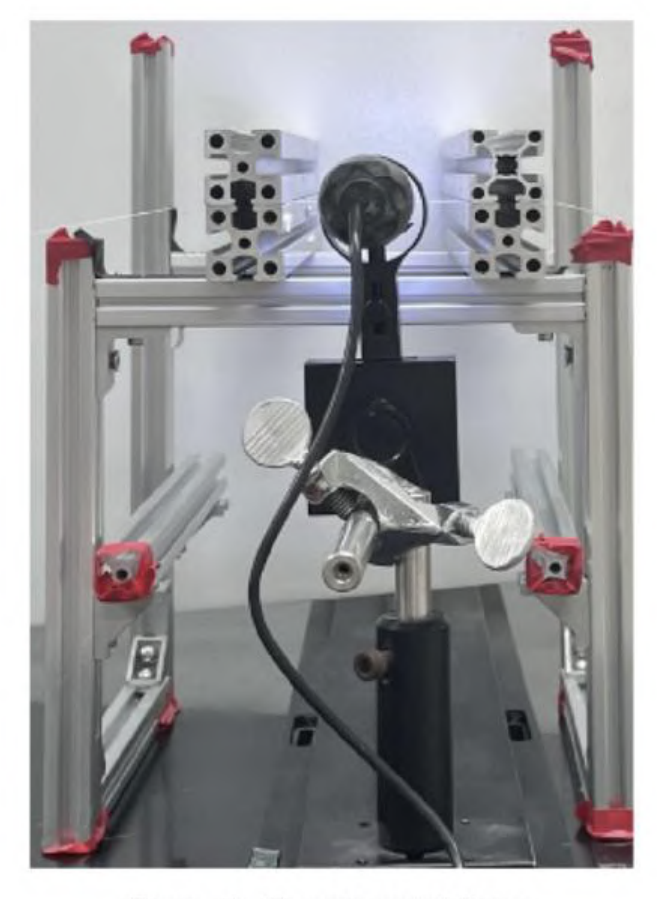
Figure 7: The saturated expansion rate (strain) of a 10x10mm piece of paper is found. It differs greatly in two perpendicular directions.

## (IV.) Pore and Fiber Sorption Aspect-Droplet Experiment

Since tracing paper is a fibrous and porous material (celluouse fiber, we concern that the mechanism of capillary of capillary imbibition in two aspects:

To clarify that the capillary mechanism is in the result of whether pore or fiber concerns, we initially did an experiment (Droplet Experiment). Here, we use a pipetmen in  $10\mu$ m amount of water (We chose such a small amount of water specifically to minimize the influence of gravity) then drop on tracing paper, forming a droplet. Then use a digital microscope to observe the droplet on hydrophobic and hydrophilic concerns.

When a water droplet comes into contact with tracing paper, the contact angle provides critical insight into the interaction between the water and the paper's fiber network. If the fibers are hydrophobic, the capillary action within the fiber web of the tracing paper is significantly reduced. This occurs because hydrophobic fibers repel water, preventing the liquid from infiltrating the microstructures of the paper. As a result, the typical capillary forces that would otherwise draw water into the fiber network are absent, leading to minimal or no swelling and a lack of observable wrinkling. Conversely, if the fibers are hydrophilic, the capillary action is more pronounced, allowing water to be absorbed into the fiber network. This absorption induces swelling as the water infiltrates and expands the cellulose fibers, leading to noticeable wrinkling and deformation of the paper.



(本人拍攝)

Figure 8: Experimental Setup

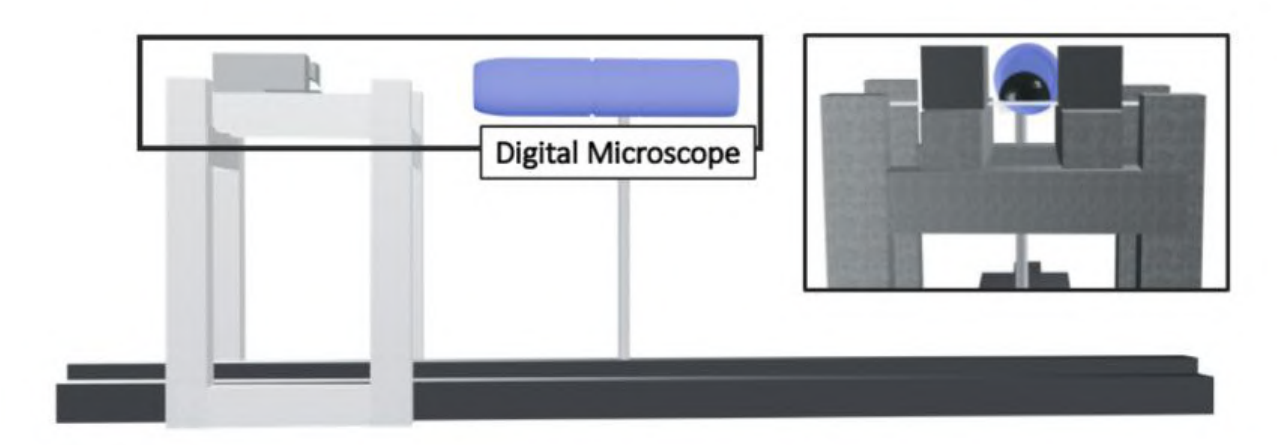


Figure 9: Experimental Setup

(本人繪製)

(本人拍攝與繪製)

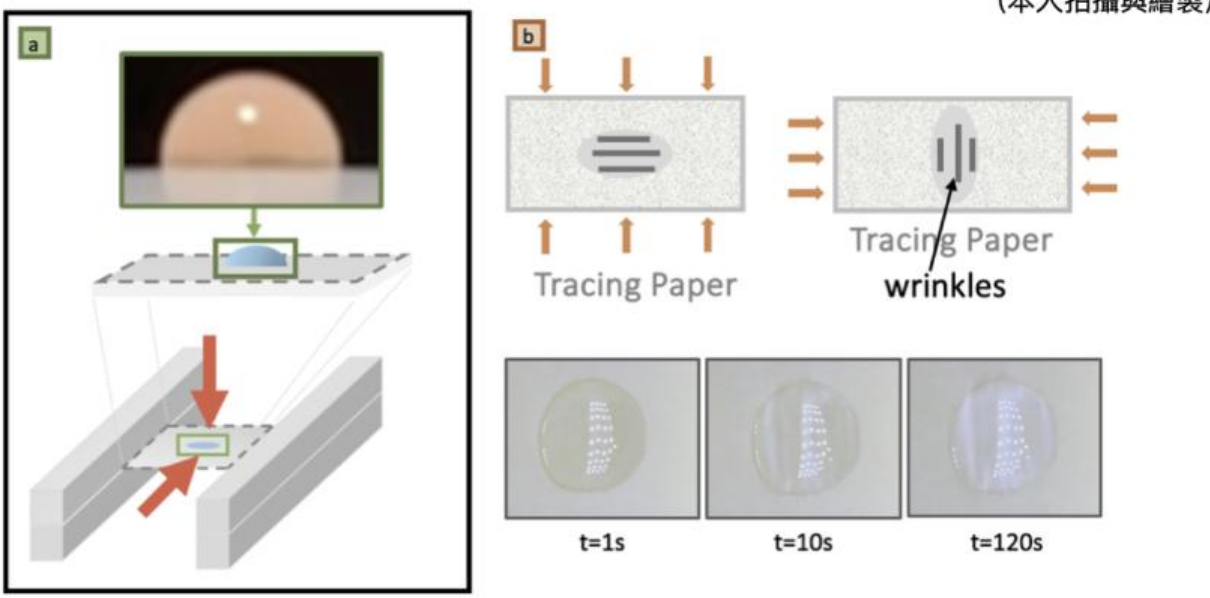


Figure 10: From fig(a) we can see that the 10 um droplet under digital microscope is hydrophobic. However, we still can see tracing paper swell after a period of time, in fig(b) below is a 10 ml of droplet on tracing paper after time, which can better show the description that mentioned. Also, we found out the curling direction of tracing paper when placed on water surface is always perpendicular to the direction of the wrinkle, which recalling to that curling direction is CD Direction that discussed further.

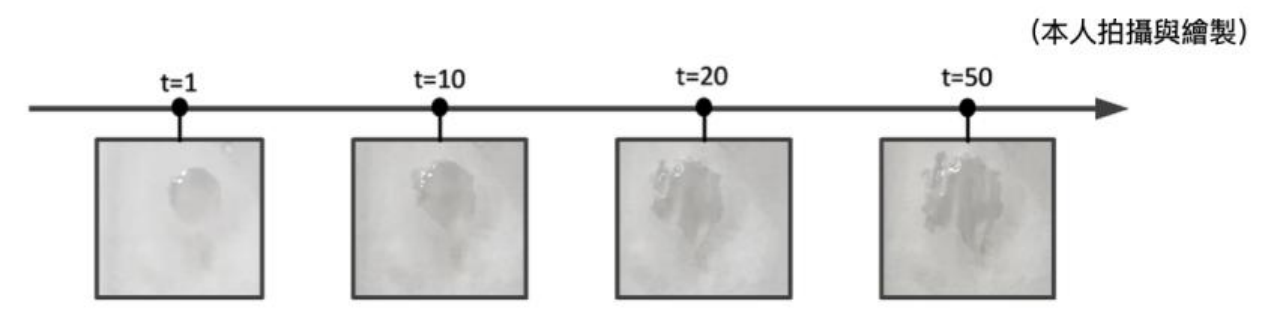


Figure 11: Here we use sandpaper to rub tracing paper then again drop a water droplet diffuse after time

According to out experimental result, we qualitatively says that tracing paper is hydrophobic on the outer layer and hydrophilic in the inner layer.

### Swelling Mechanism

#### Introduction

The swelling mechanism of tracing paper is a complex interplay between its hydrophobic outer layer and hydrophilic inner layers. Initial water resistance is overcome through cap-

illary action, allowing water to reach the absorbent cellulose fibers beneath the surface. This process is primarily driven by pore sorption, suggesting that while the outer layer repels water, the inner structure's hydrophilicity leads to eventual swelling. Understanding this mechanism, particularly the role of coatings and the dual-layer structure, is essential for applications where the moisture resistance and swelling behavior of tracing paper are critical factors.

#### Observations and Hydrophobic Nature of Tracing Paper

In recent droplet experiments conducted on tracing paper, a unique swelling mechanism was observed that did not align with typical water absorption behaviors seen in other cellulose-based papers. Both vertical and perpendicular applications of water droplets revealed that the water front did not diffuse after a prolonged period, indicating a distinct interaction between the tracing paper's surface and water. This behavior highlights the hydrophobic characteristics of the outer layer of tracing paper, which plays a crucial role in its initial resistance to swelling.

The hydrophobicity of tracing paper is primarily due to its outer layer, which has been treated or coated to repel water. Hydrophobic surfaces typically resist water penetration, leading to delayed or minimal swelling. This behavior can be explained through the mechanism of hydrogen bonding, which governs the interaction between water and cellulose fibers. According to Klemm et al. (1998), the hydrogen bonds within cellulose fibers are crucial in determining water absorption properties. In cellulose, the hydroxyl groups form hydrogen bonds with water molecules, facilitating water absorption and subsequent swelling. However, when a hydrophobic coating is applied to the surface, these interactions are significantly hindered, preventing immediate swelling upon contact with water.

#### Inner Hydrophilic Layer and Capillary Action

Despite the initial resistance due to hydrophobicity, tracing paper does eventually swell over time, indicating that its inner layers are hydrophilic. This delayed swelling suggests that water penetration is not primarily due to the fibers themselves but rather through capillary action within the pores of the paper.

This capillary action, driven by the pore sorption mechanism described by the Richardson equation, allows water to be drawn into the microscopic pores of the paper, bypassing the hydrophobic barrier. Initially, it was assumed that the swelling mechanism was dominated by fiber sorption, where water enters the fiber through parallel cylindrical capillaries, leading to swelling. However, since tracing paper exhibits hydrophobic properties,

this fiber sorption mechanism appears insufficient. The hydrophobic nature suggests that while the outer layer of the paper repels water, the inner layers may possess hydrophilic characteristics. As water penetrates through capillary action into these inner layers, it causes the cellulose fibers to absorb water, resulting in swelling.

#### Coating and Hydrophobicity Considerations

The hydrophobic nature of the outer layer in tracing paper is often a result of specific treatments or coatings applied during its manufacturing. According to Kjellgren (2007), the barrier properties of greaseproof paper, including tracing paper, are significantly influenced by polymer coatings applied to enhance their resistance to moisture and grease. These coatings contribute to the paper's hydrophobic characteristics, preventing water from penetrating the surface and thus delaying swelling. However, once the water overcomes this barrier, likely through capillary action into the pores, it reaches the inner, hydrophilic layers, where it can cause swelling.

## III. Qualitative and Quantitative

### (I.) Mechanism Explanation

#### **Diffusion Model Discussion**

It is argued that capillary effect is not involved by showing that surfactants does not affect the curvature (Reyssat and Mahadevan 2011). However, it should be noted that surfactant molecules cannot penetrate cellulose surfaces in aqueous solutions (Penfold et al. 2007). Since surfactant molecules cannot affect the water that goes into the paper, the capillary effects must not be ruled out. Moreover, we could see later (9) that the mathematical representation of Fick's law is merely a limiting case of the Richards equation. This suggests a broader view be obtained when capillary effect is considered, rather than assuming a limiting case.

#### Capillary Model Discussion

The capillary model proposed by (Washburn 1921) is well-known and is applicable to many cases of porous materials. However, (Reyssat and Mahadevan 2011) proposed that this model failed to account for the whole phenomenon. Literature (Huinink, Ruijten, and Arends 2016; Perez-Cruz, Stiharu, and Dominguez-Gonzalez 2017) shows that a key assumption of the Washburn law is the binary distribution of water content in a porous media, and we think this is why the model fails to explain the results. To improve on

this, (Huinink, Ruijten, and Arends 2016) proposed a model that accounts for the gradual transition of water and air regime, allowing non-sharp boundary of water and air.

To begin the discussion of capillary model, describing how water moves in paper is critical. To quantitatively describe how much water is in the paper at a specific location z and time t, we follow (Huinink, Ruijten, and Arends 2016)volumetric water content as the ratio of water and the total volume,

We define the volumetric water content as the ratio of water and the total volume thebibliography.

$$\theta = \frac{V_{H_2O}}{V_{H_2O} + V_{cellulose}} \tag{1}$$

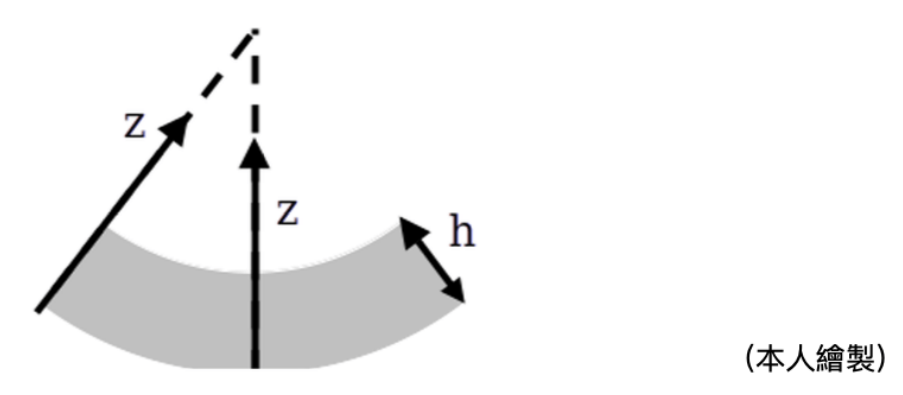


Figure 12: The coordinate axis of the paper. The origin of z axis is set at the water surface, and the direction is perpendicular to local tangent plane of paper.

Here, Fig. shows that the water content is dependent of z, but not in the x and y axis of paper because of symmetry. Water content is seen to linearly increase the strain of paper without producing recovering stress. According to **Nissan1976**, Young's modulus decreases exponentially with volumetric water content. The decay coefficient may be different for various materials, and it is fitted in our case to be -24.32.

$$E(\theta) = E_0 e^{-24.32\theta} \tag{2}$$

By capillary reasoning, Richards equation can be used to model water penetration through porous media **Huinink2016**.

$$\frac{d\theta}{dt} = D_0 \frac{d}{dz} \left( \theta^n \frac{d\theta}{dz} \right) \tag{3}$$

in which  $D_0$  is called "diffusivity" for convenience. It should be noted that  $D_0$  is of

capillary nature, and there is no diffusion involved. The exponent n takes a value of,

$$n = 1 + \frac{2\lambda}{\lambda} \tag{4}$$

Where  $\lambda$  is the pore distribution index **Huinink2016**, which is smaller when the pore sizes are near, we arrive that,

$$D = D_0 \theta^n, \quad n = 2 + \frac{1}{\lambda} \tag{5}$$

 $D_0$  can also be written explicitly, when cylendrical pores is assumed

$$D_0 = \frac{\gamma \cos \alpha r}{4\mu\lambda} \tag{6}$$

When trying to fit the experimental data, (Perez-Cruz, Stiharu, and Dominguez-Gonzalez 2017) uses an exponential value of 1.1, which is contradictory against what (Huinink, Ruijten, and Arends 2016) had proposed. We think it may illuminate the fact that the assumption of cylindrical pore does not apply.

#### Richard's Derivation

The path of **Huinink2016** would be followed to derive Richards equation. The law of mass conservation is well-known,

$$\frac{\partial \theta}{\partial t} = -\frac{\partial q}{\partial x} \tag{7}$$

Since paper is a porous media, Darcy's law applies,

$$\frac{\partial \theta}{\partial t} = \frac{\partial}{\partial x} \left( \frac{k(\theta)}{\mu} \left( \frac{\partial p(\theta)}{\partial x} + \rho g \hat{z} \right) \right) \tag{8}$$

Where k is the permeability involved in Darcy's law,  $\mu$  is the liquid viscosity, p is the pressure in the pore,  $\rho$  is the liquid density, g is the gravitational acceleration,  $\hat{z}$  is the unit vector in the direction of gravity. It is known that the pressure can be written as

$$p = p_0 - p_c(\theta) \tag{9}$$

Where  $p_0$  is the equilibrium pressure of liquid and air,  $p_c$  is the pressure provided by capillary action. Rewriting the equation and ignoring gravity,

$$\frac{\partial \theta}{\partial t} = -\frac{\partial}{\partial x} \left( \frac{k(\theta)}{\mu} \left( \frac{\partial p_c(\theta)}{\partial x} \right) \right) \tag{10}$$

Packing the coefficients,

$$\frac{\partial \theta}{\partial t} = \frac{\partial}{\partial z} \left( D \frac{\partial \theta}{\partial z} \right) \tag{11}$$

With the value of D given by,

$$D = -\frac{k}{\mu} \frac{\partial p_c}{\partial \theta} \tag{12}$$

Given the simplified Brooks-Corey relationship,

$$p_c(\theta) = p_{c0}\theta^{-\frac{1}{\lambda}}, \quad k(\theta) = k_{\text{max}}\theta^{3+\frac{2}{\lambda}}$$
(13)

#### Mere Limiting Case-Diffusive Mathematical Formula

It is seen now that the diffusive mathematical formula (Fick's law) can be seen as a mere limiting case of the Richards equation (10) at late time, when the water content is close to saturation everywhere.

$$\frac{\partial \theta}{\partial t} = D_{\text{sat}} \frac{\partial^2 \theta}{\partial z^2}, \quad D_{\text{sat}} = D_0 \theta_{\text{sat}}^n$$
 (14)

The boundary condition at the bottom (z=0) states that paper remain saturated in contact with water; at the top there may be effects of evaporation, which is not considered significant given the time duration of the problem. However, we consider it critical as it can account for the deviation for the uncurling phase.

$$\theta(0,t) = \theta_{sat}, \quad \frac{d\theta}{dz}(h,t) = \frac{q}{AD_0}$$
 (15)

 $\theta_{sat} = 0.33$  is the saturated volumetric water content, h is the paper thickness, q is the volumetric evaporation rate, A is the surface area of paper.  $\theta_{sat}$  is measured by weighing the paper before and after dipping in water, and converted to volumetric ratio by density of water and paper, both measured in a short enough duration of time.

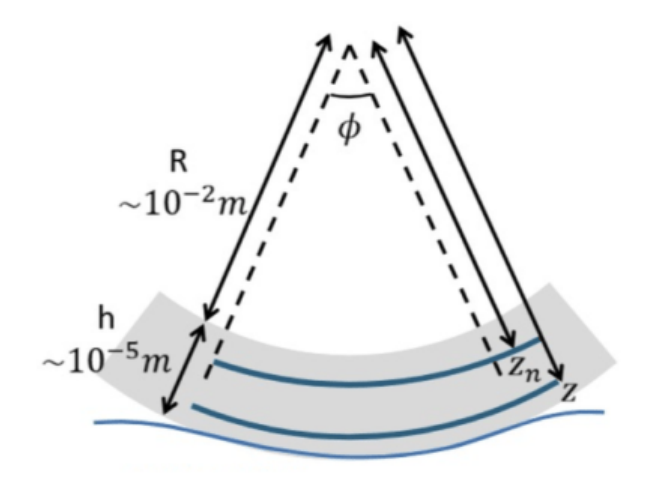


Figure 13: The geometry of curling paper.

(本人繪製)

For quantitative prediction of curvature, we consider the net strain  $(\epsilon)$  and stress  $(\sigma)$  produced by curvature being canceled by the strain introduced by water penetration **Reyssat2011**.

$$\epsilon_{\kappa} = \kappa(z - z_n) \tag{16}$$

$$\epsilon_{\theta} = \epsilon_{sat} \frac{\theta}{\theta_{sat}} \tag{17}$$

$$\sigma = E(\epsilon_{\kappa} - \epsilon_{\theta}) \tag{18}$$

Where  $\kappa$  is the curvature, z is the position in the axis of paper thickness,  $z_n$  is the position of neutral layer, E is the Young's modulus. Assuming quasi-static process, we arrive at the prediction **Reyssat2011**.

$$\kappa = \frac{I_1 I_{\phi 0} - I_0 I_{\phi 1}}{I_1^2 - I_0 I_2} \tag{19}$$

$$I_0 = \int_0^h E \, dz, \quad I_1 = \int_0^h Ez \, dz, \quad I_2 = \int_0^h Ez^2 \, dz$$
 (20)

$$I_{\phi 0} = \int_0^h E \epsilon_\phi \, dz, \quad I_{\phi 1} = \int_0^h E z \epsilon_\phi \, dz \tag{21}$$

Under this model, curvature is dictated by water content. Richards equation can only be used to predict normalized curvature **Perez-Cruz2017**. We follow the path and use only maximum curvature to adjust this. It is seen that Richards equation fits the curling phase really well, but cannot predict the uncurling phase (Fig. 2). Since at late time

the diffusivity approaches a constant, we can use Fick's law to approximate late time behavior. We will use exponential function to approximate Fick's law **Reyssat2011**,

$$\kappa(t) \approx C \frac{\epsilon}{h} e^{-\frac{\pi^2 D t}{4h^2}} \tag{22}$$

Where  $C \approx 1.33$ , D is the late time diffusivity. It is seen that it fit the data nicely.

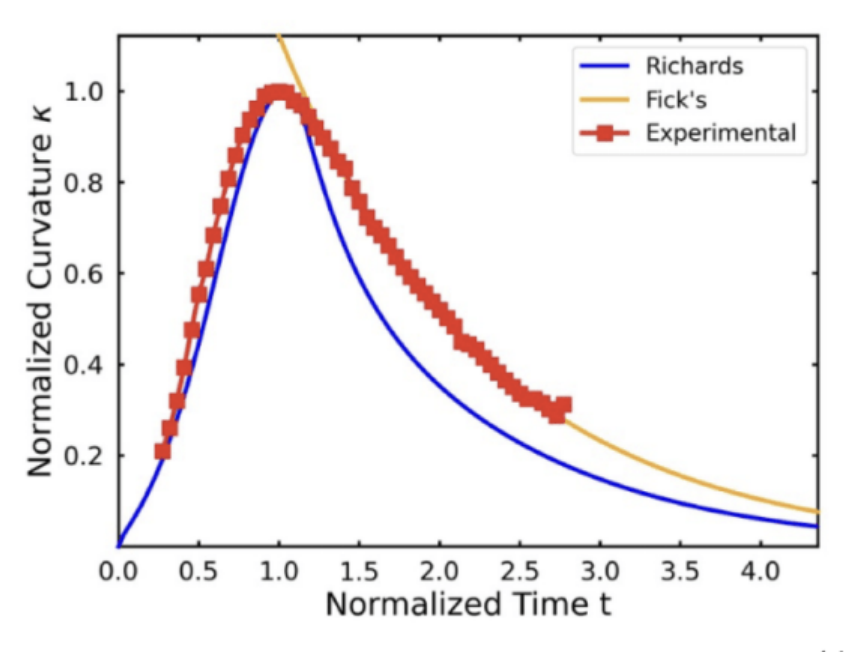


Figure 14: Fitting of Data

(本人分析輸出擷取)

## (II.) Finite Difference Method - Richards Simulation

In this work, we apply the forward difference method to calculate the solution at the next time step. For the linear diffusion equation, the solution is considered stable when the following condition holds:

$$\frac{D_0^2 \Delta t}{\Delta z^2} \le \frac{1}{2} \tag{23}$$

Although it is uncertain whether this stability criterion applies in the nonlinear scenario, it serves as a useful reference point.

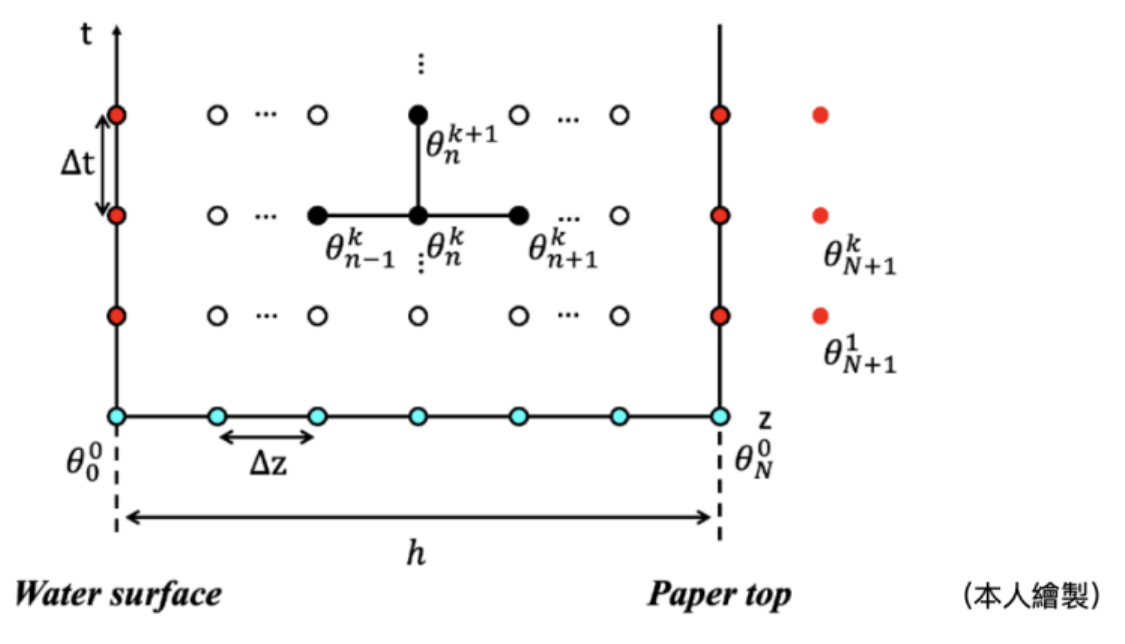


Figure 15: Finite Difference Method-Forward Difference

Moving forward, we consider the Robin boundary condition. Unlike Dirichlet boundary conditions, which are typically applied at n + 1 = N, the Robin boundary condition requires an extension to n = N, where virtual points are introduced to simulate the boundary condition. The Robin boundary condition can be expressed as:

$$\left. \frac{\partial \theta}{\partial z} \right|_{z=h} = -c\theta \tag{24}$$

When discretized, the above boundary condition becomes:

$$\frac{\theta_{N+1}^k - \theta_{N-1}^k}{2\Delta z} = -c\theta_N^k \tag{25}$$

which leads to the following expression for  $\theta_{N+1}^k$ 

$$\theta_{N+1}^k = -2c\Delta z \theta_N^k + \theta_{N-1}^k \tag{26}$$

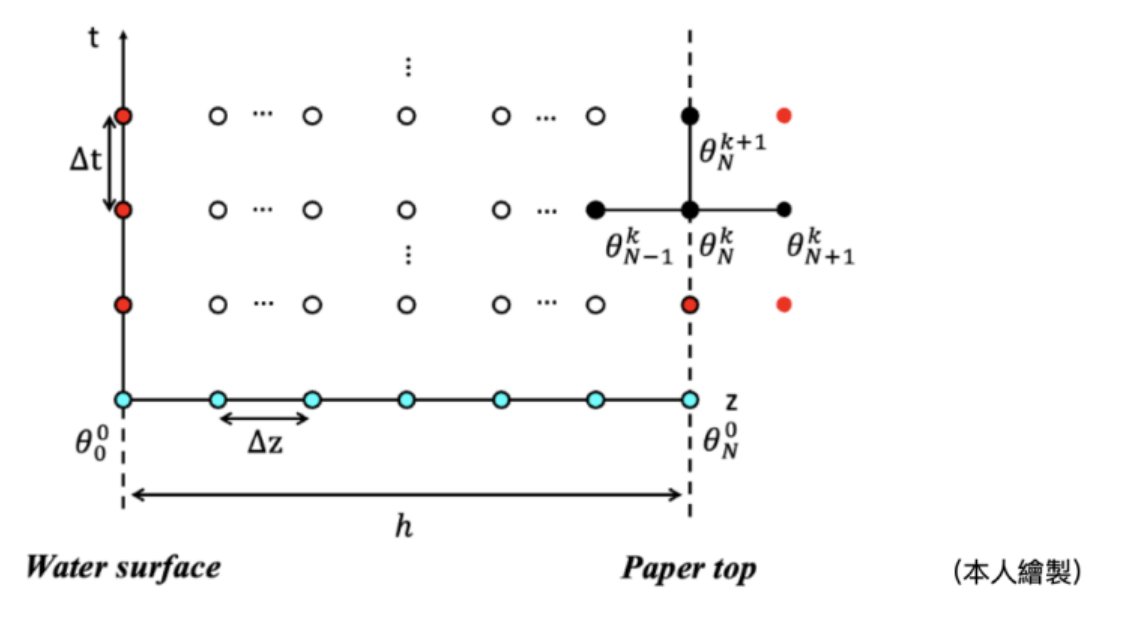


Figure 16: Finite Difference Method-Robin Boundary Condition(Robin BC)

This method is derived from the reference material. Now, we present the derivation of the equation for our case, based on Richards' equation:

$$\frac{\partial \theta}{\partial t} = D_0 \theta^{m-1} \left( m \left( \frac{\partial \theta}{\partial z} \right)^2 + \theta \frac{\partial^2 \theta}{\partial z^2} \right). \tag{27}$$

Using the forward difference scheme to approximate the time derivative  $\frac{\partial \theta}{\partial t}$  and the central difference scheme for the spatial derivatives, we obtain:

$$\frac{\theta_n^{k+1} - \theta_n^k}{\Delta t} = D_0 \left(\theta_n^k\right)^{m-1} \left( m \left( \frac{\theta_{n+1}^k - \theta_{n-1}^k}{2\Delta z} \right)^2 + \theta_n^k \left( \frac{\theta_{n+1}^k - 2\theta_n^k + \theta_{n-1}^k}{\Delta z^2} \right) \right) \tag{28}$$

Rearranging this expression, for all n < N - 1 we get:

$$\theta_n^{k+1} = \theta_n^k + \frac{\Delta t}{\Delta z^2} D_0 \left(\theta_n^k\right)^{m-1} \left(\frac{m}{4} \left(\theta_{n+1}^k - \theta_{n-1}^k\right)^2 + \theta_n^k \left(\theta_{n+1}^k + \theta_{n-1}^k\right) - 2\left(\theta_n^k\right)^2\right)$$
(29)

We impose the Dirichlet boundary condition at n = 0 as:

$$\theta_0^k = \theta_{\text{sat}} = 0.25 \tag{30}$$

For the Robin boundary condition, using the virtual point relation derived earlier, we have:

$$\theta_{N+1}^k = -2c\Delta z \theta_N^k + \theta_{N-1}^k \tag{31}$$

Thus, at n = N, we have the following equation:

$$\theta_N^{k+1} = \theta_N^k + \frac{\Delta t}{\Delta z^2} D_0 \left(\theta_N^k\right)^{m-1} \left(\frac{m}{4} \left(-2c\Delta z \theta_N^k\right)^2 + \theta_N^k \left(2\theta_{N-1}^k - 2c\Delta z \theta_N^k\right) - 2\left(\theta_N^k\right)^2\right)$$
(32)

If c = 0, the Robin boundary condition reduces to a Neumann boundary condition, and the equation simplifies to:

$$\theta_N^{k+1} = \theta_N^k + \frac{\Delta t}{\Delta z^2} D_0 \left(\theta_N^k\right)^m \left(2\theta_{N-1}^k - 2\theta_N^k\right) \tag{33}$$

The issue with the original approximating scheme arises when the initial condition (IC) is applied, leading to zero results. Specifically, the imposed initial condition is:

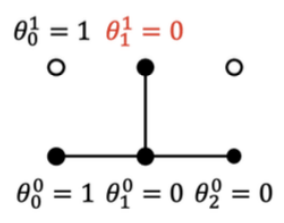
$$IC: egin{cases} heta(0,0) = heta_{\mathrm{sat}}, & \forall z = 0, \ heta(z,0) = 0, & \forall z \neq 0. \end{cases}$$

This problem occurs due to the form of the discretized equation:

$$\theta_n^{k+1} = \theta_n^k + \frac{\Delta t}{\Delta z^2} D_0 \left(\theta_n^k\right)^{m-1} \left(\frac{m}{4} \left(\theta_{n+1}^k - \theta_{n-1}^k\right)^2 + \theta_n^k \left(\theta_{n+1}^k + \theta_{n-1}^k\right) - 2\left(\theta_n^k\right)^2\right)$$
(34)

At the first time step k=0 and for n=1, the stencil fails to propagate the boundary condition outwards. Specifically, for  $\theta_1^1$ , the resulting value is zero due to the initial zero conditions at n=1, and this pattern persists for all t>0, leading to a failure to propagate the boundary condition properly. To resolve this, we assume that the variation at the boundary is small enough so that the following approximations hold:

$$\theta_n^k \approx \frac{1}{2} \left( \theta_{n-1}^k + \theta_{n+1}^k \right), \quad \text{and} \quad \theta_N^k \approx \theta_{N-1}^k$$
 (35)



Using these assumptions, we reformulate the forward finite difference approximating scheme for all  $n \leq N-1$  as:

$$\theta_n^{k+1} = \theta_n^k + \frac{\Delta t}{\Delta z^2} D_0 \left( \frac{1}{2} \left( \theta_{n-1}^k + \theta_{n+1}^k \right) \right)^{m-1} \left( \frac{m}{4} \left( \theta_{n+1}^k - \theta_{n-1}^k \right)^2 + \theta_n^k \left( \theta_{n+1}^k + \theta_{n-1}^k \right) - 2 \left( \theta_n^k \right)^2 \right)$$
(36)

At the boundary point n = N, we have the following modified equation for n = N:

$$\theta_N^{k+1} = \theta_N^k + \frac{\Delta t}{\Delta z^2} D_0 \left(\theta_N^k\right)^m \left(2\theta_{N-1}^k + \theta_N^k \left(mc^2 \Delta z^2 - 2c \Delta z - 2\right)\right), \tag{37}$$

The boundary condition remains:

$$\theta_0^k = \theta_{\text{sat}} \tag{38}$$

The initial condition is:

$$IC: \begin{cases} \theta_0^0 = \theta_{\text{sat}}, & \forall n = 0, \\ \theta_n^0 = 0, & \forall n \neq 0 \end{cases}$$

This reformulated scheme resolves the issue of zero propagation by allowing the boundary condition to propagate correctly into the interior points, ensuring that the boundary effects are transmitted throughout the domain as time progresses.

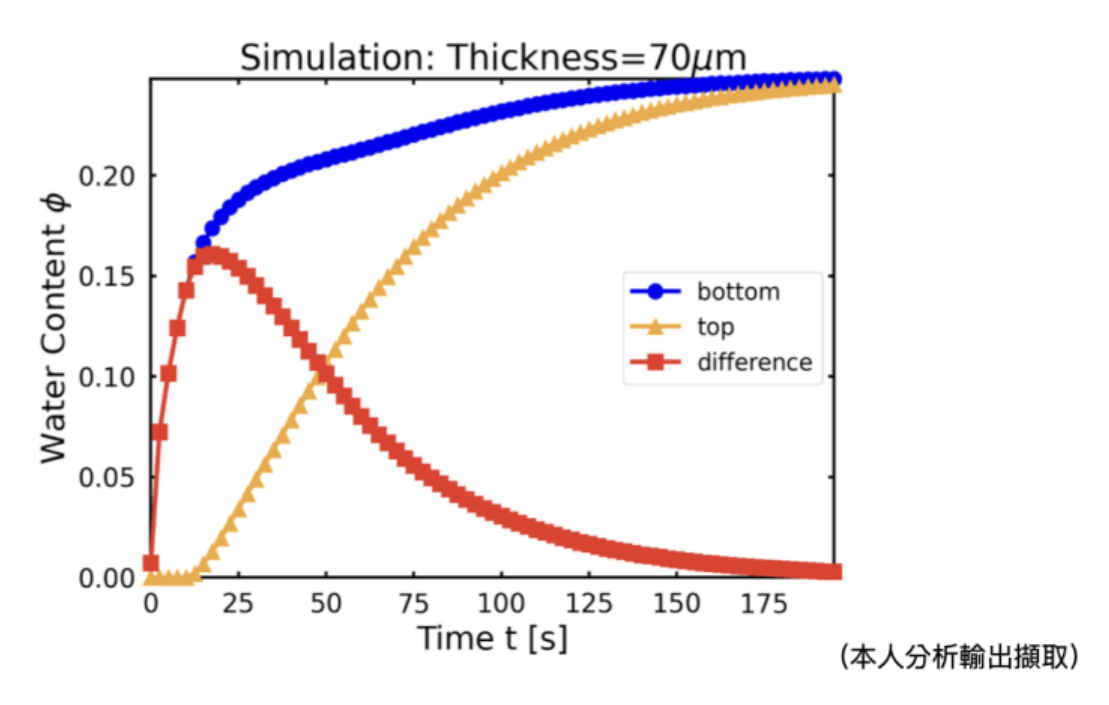


Figure 17: Richard's Simulation-Without Evaporation

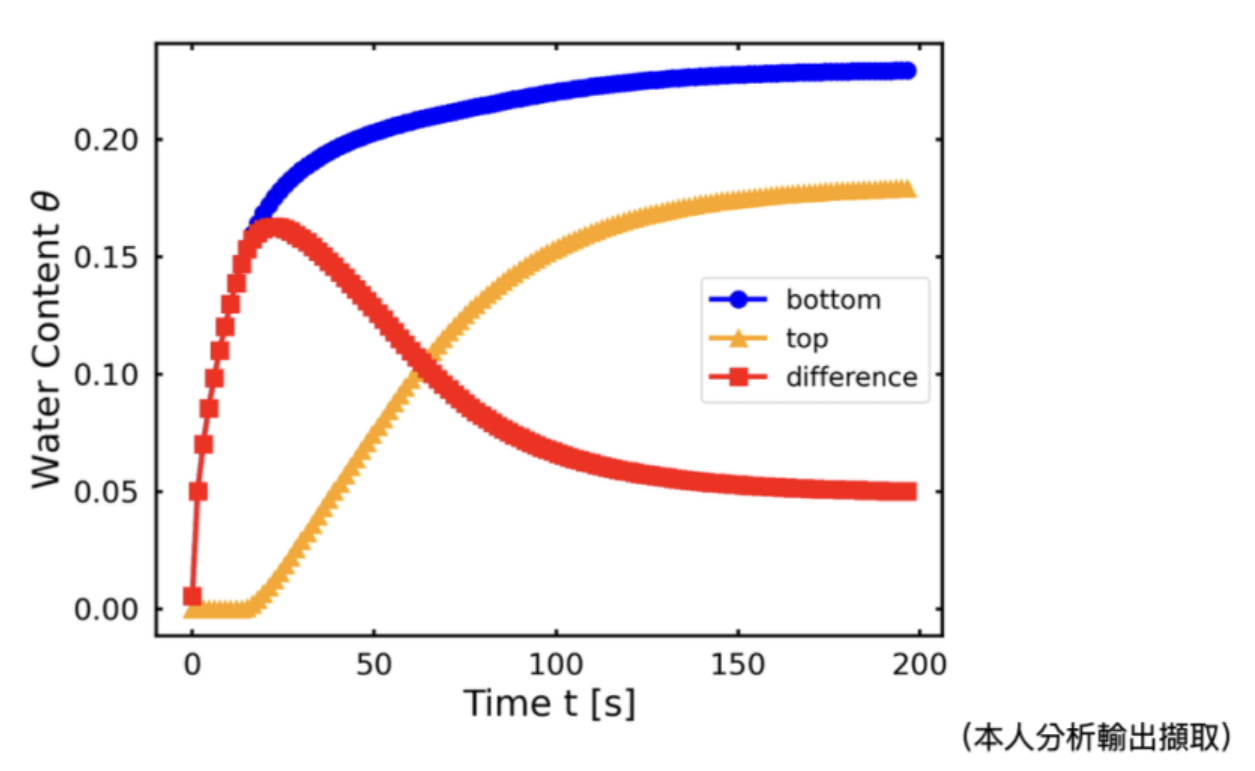


Figure 18: Richard's Simulation-With evaporation

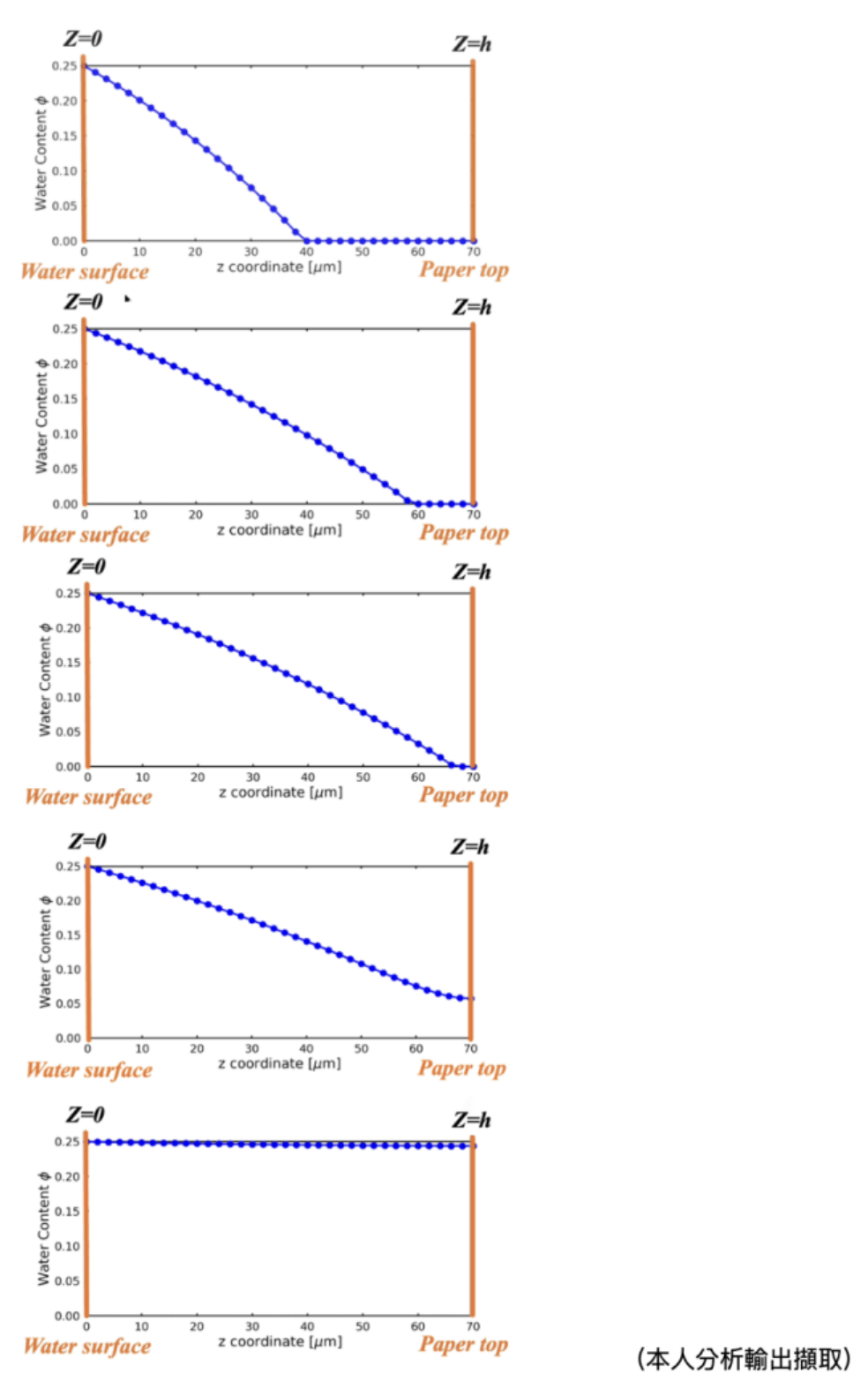
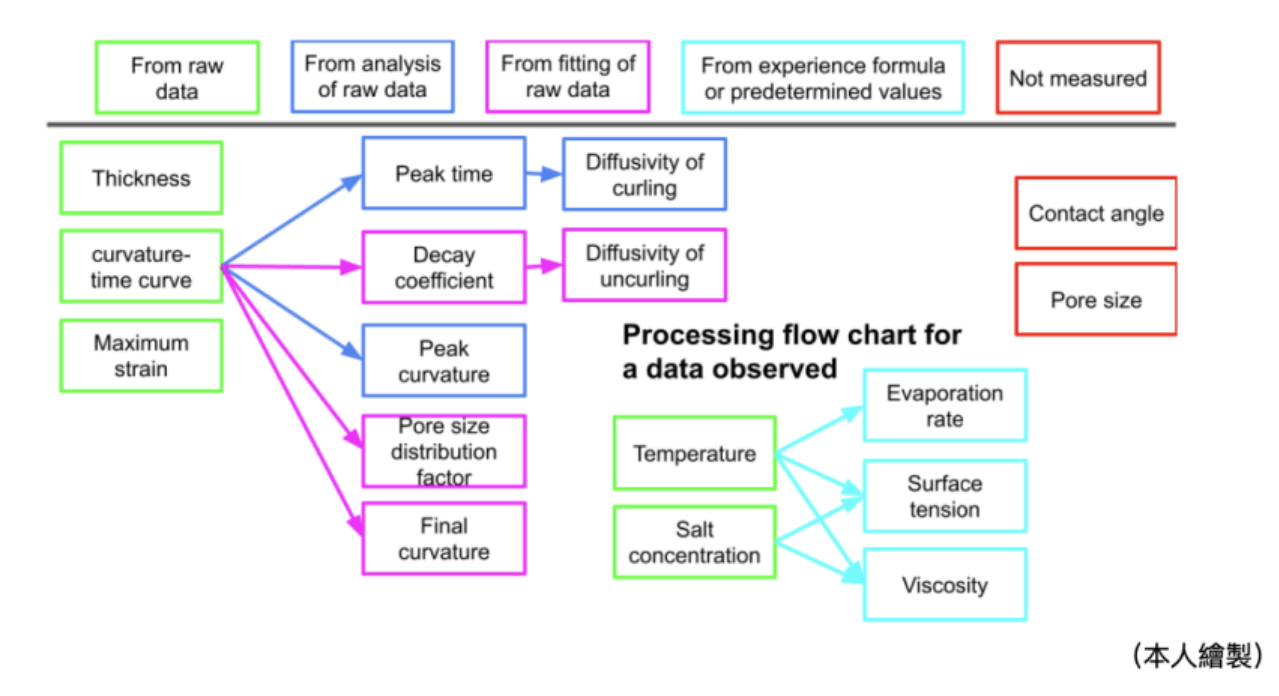


Figure 19: Dynamic Simulation of water content of Richard's Equation in layers of tracing paper

### (IV.)Parameters Discussion



Paper dimension is fixed to be 10x10mm in length and width, and  $87.15\mu$ m in thickness if not specified. Paper thickness. By normalization of Richards equation, we see the time scale is (Perez-Cruz, Stiharu, and Dominguez-Gonzalez 2017),

$$\tau = \frac{h^2}{D_0 \phi_{sat}} \tag{39}$$

and the curvature scale is,

$$\kappa = \frac{\epsilon_{sat}}{h} \tag{40}$$

By simulation methods, we can deduce that the peak time and curvature is directly proportional to the scales,

$$t_{max} = 0.62\tau, \quad \kappa_{max} = 1.1\kappa \tag{41}$$

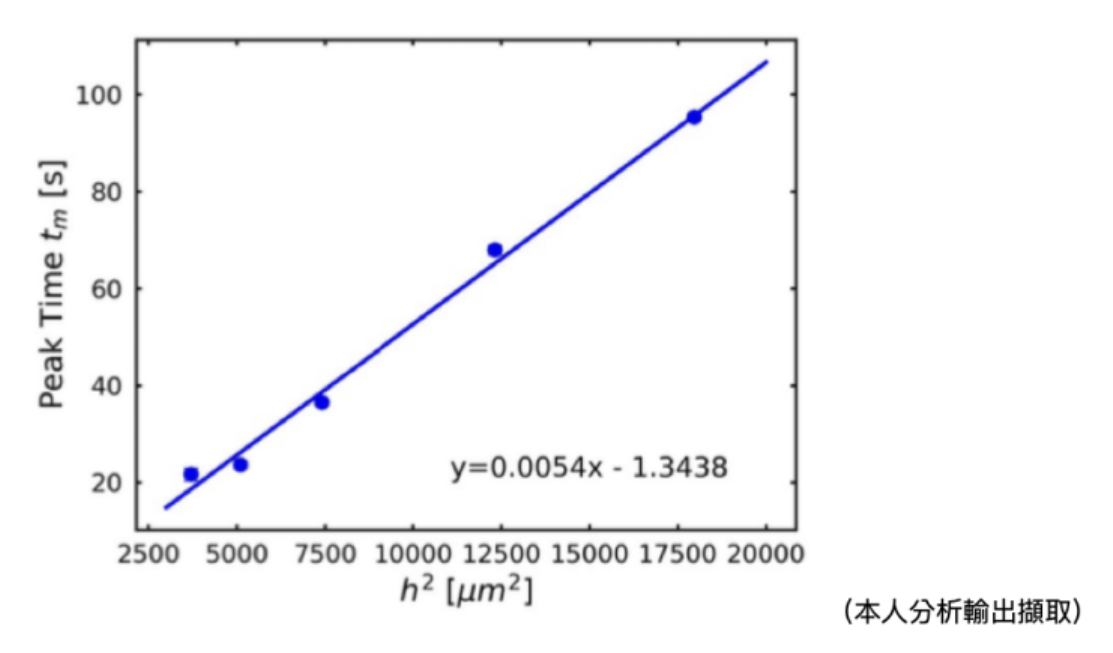


Figure 20: Linear relationship with peak curvature and reciprocal of thickness.

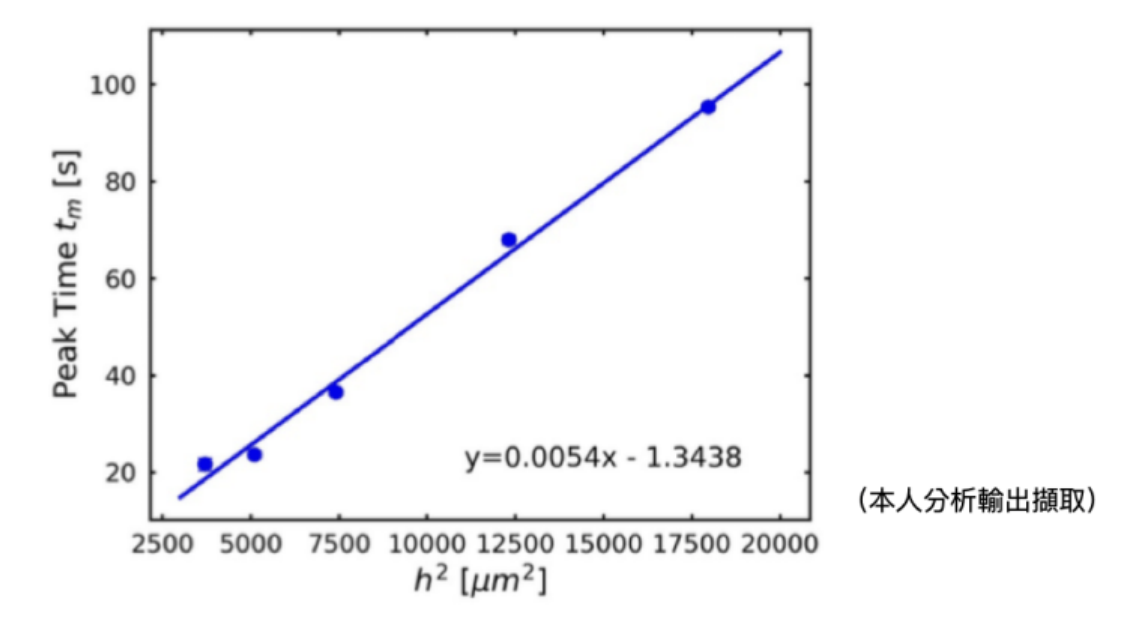


Figure 21: Linear relationship between peak time and thickness squared.

## (V.)Temperature and Evaporation

Temperature itself affects a lot of factors, including Young's modulus, surface tension, viscosity, and evaporation rate. The absolute value of Young's modulus does not matter,

since we assumed a quasi-static process. For surface tension and viscosity, it is mentioned that their ratio affects the diffusivity linearly. It is previously measured that temperature dependence of surface tension and viscosity of water can be described by the following formulae:

$$\gamma = a \left(\frac{T_c - T}{T_c}\right)^b \left(1 - c \left(\frac{T_c - T}{T_c}\right)\right), \tag{42}$$
 
$$a = 0.2358, \quad b = 1.256, \quad c = 0.625, \quad T_c = 647.15 \, \mathrm{K}, \quad 273.01 \, \mathrm{K} \le T \le 647 \, \mathrm{K}$$

$$\mu = Ae^{B/T} + CT + DT^2,\tag{43}$$

$$A = 1.86 \times 10^{-14}$$
,  $B = 4209$ ,  $C = 0.04527$ ,  $D = -3.38 \times 10^{-5}$ ,  $273 \text{ K} \le T \le 643 \text{ K}$ 

Therefore we can plot diffusivity at different temperatures against their corresponding ratios. The linear relationship is again seen, yet an apparent transition appears in the middle. The uncurling speed, which is approximated by Fick's law, also has a similar linear trend, but with no transition involved. Rising temperature also increases peak curvature, which indicates yet another limitation of the theory. Curling speed is also increased at high temperature, indicating the softening of paper.

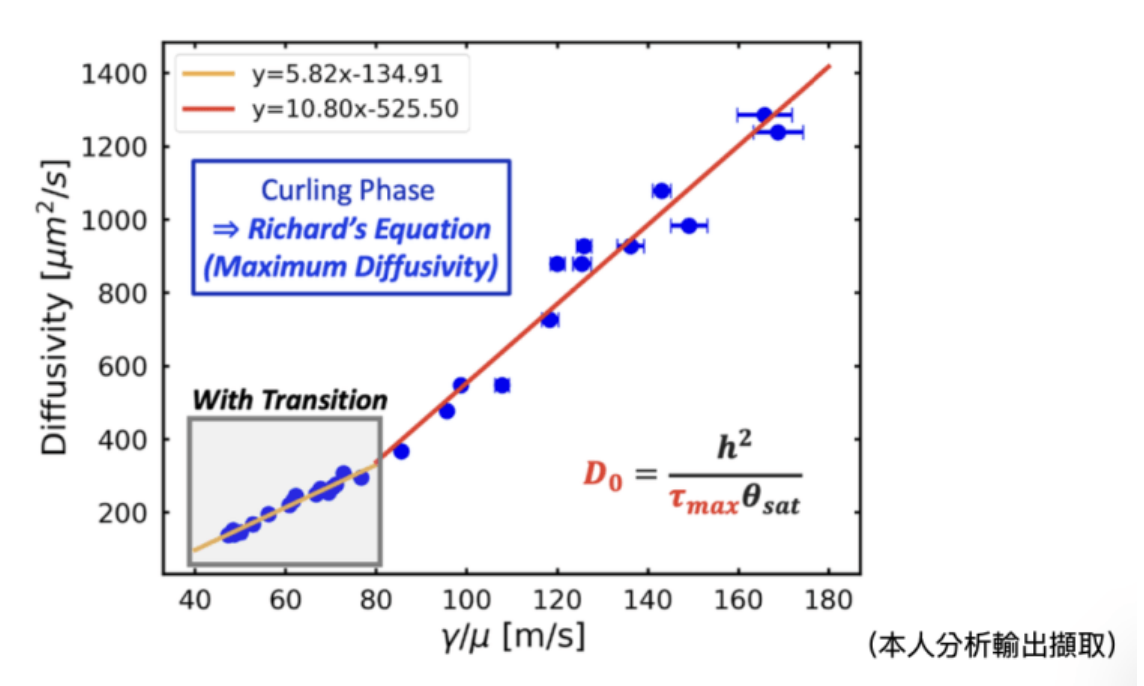


Figure 22: Linear relationship of maximum diffusivity, obtained by peak time, between ratio of surface tension and viscosity, with a transition.

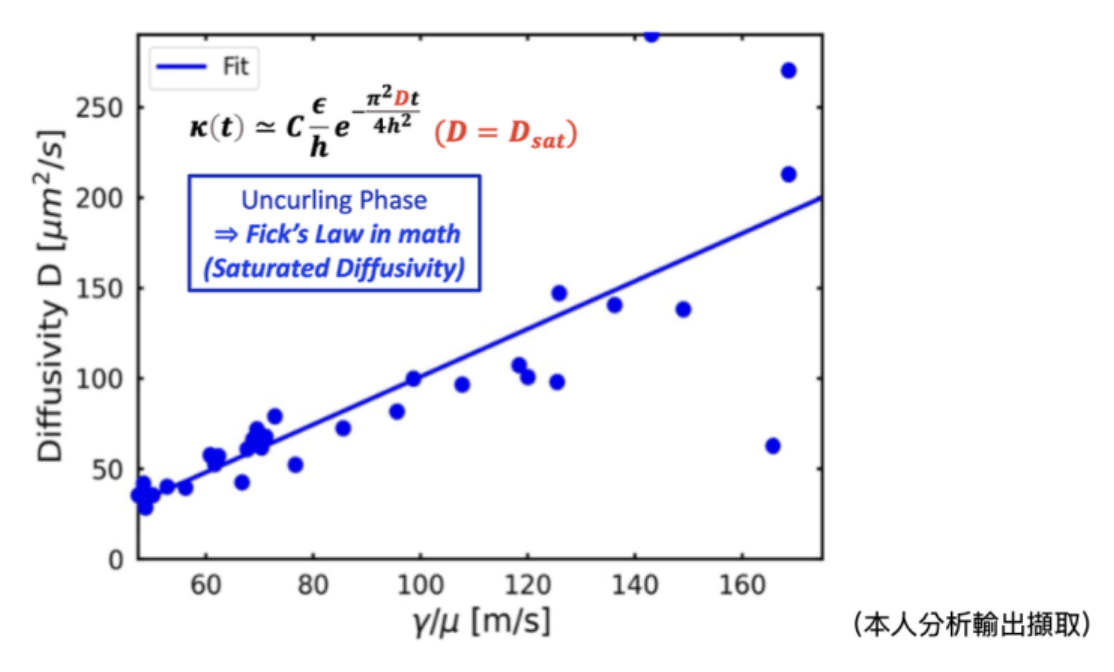


Figure 23: Linear relationship between saturated diffusivity, obtained by uncurling speed, and ratio of surface tension and viscosity.

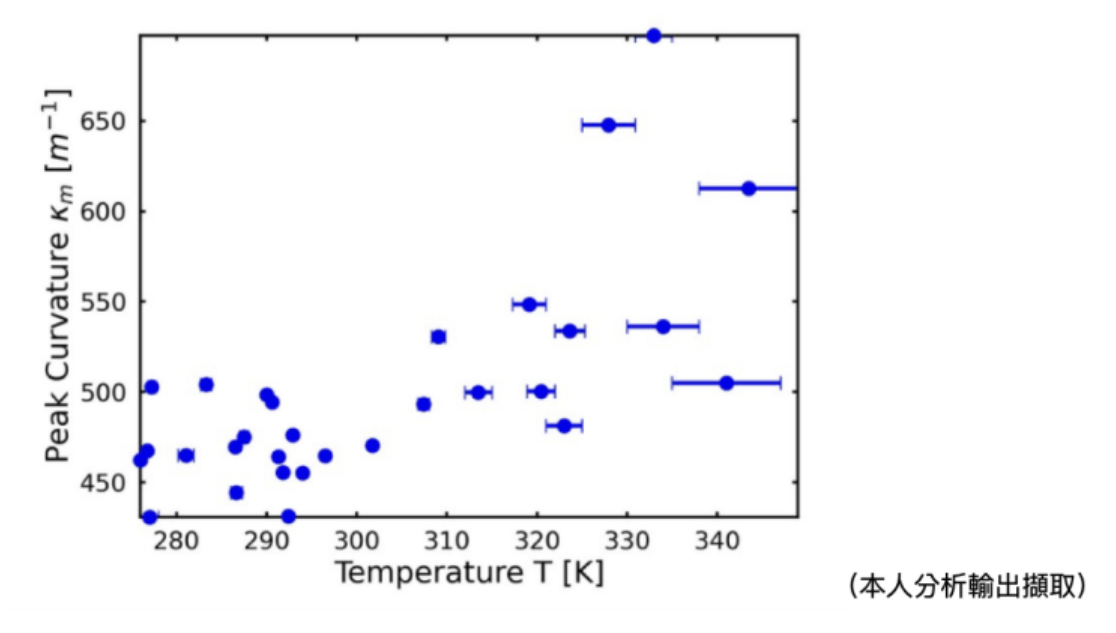


Figure 24: Relationship between peak curvature and temperature, measured in Kelvins.

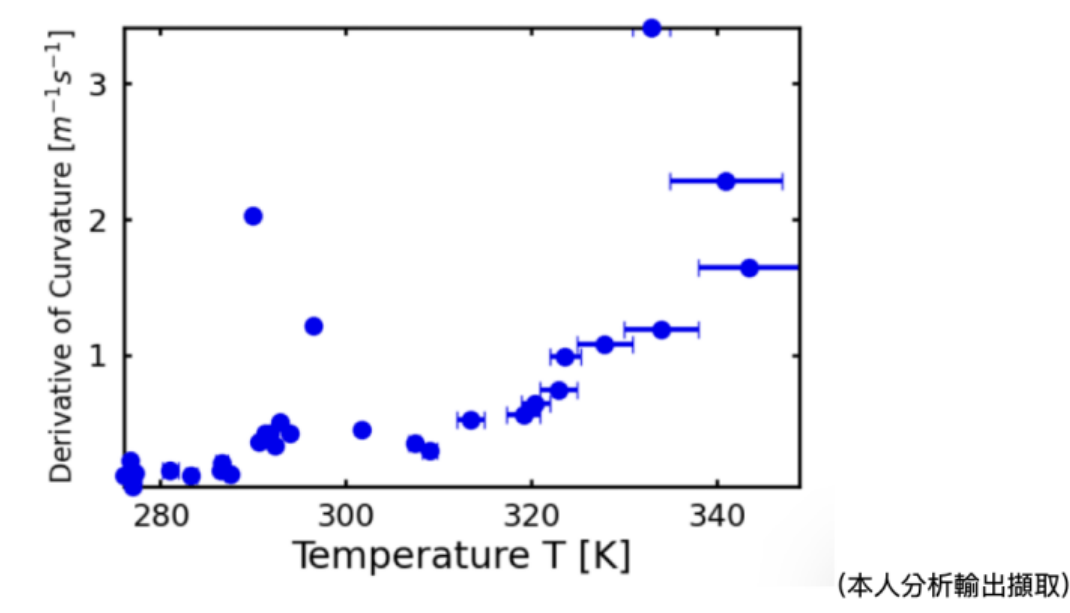


Figure 25: Relationship between curling speed and temperature. Curling speed obtained by averaging the derivative of curvature from start to peak time.

Moreover, it is observed that at high temperatures (50 degrees Celsius) the tracing paper will not uncurl to zero curvature. By setting a flux boundary condition on top in the simulation, it is seen that a constant water content difference in the top and bottom half layer of paper is reached at late time, and therefore curvature approaches a constant. The precise value of the evaporation rate is measured and fitted with an exponential function. It is well-known that the steady-state solution of Fick's law with flux boundary conditions is linear in space, and by this distribution, the final value of curvature can be proven to be:

$$\kappa_{\text{final}} = \frac{\epsilon_{\text{sat}} q}{\theta_{\text{sat}} A D_0},\tag{44}$$

which shows a linear dependence on evaporation rate. However, the experimental results show a clear transition. We think, along with the transition previously seen, that it is related to the pore depth viewed from the top. The evaporation rate needs to be high enough for the water molecules to escape the deep pores. This fact is supported by comparing the slope of the two lines. In high evaporation rates, the slope is closer to the theory prediction, indicating less obstruction.

## Derivation of Final Curvature from Fick's Second Law with Flux Boundary Conditions

Fick's Second Law in one dimension describes the diffusion of moisture through the paper:

$$\frac{\partial \theta}{\partial t} = D_0 \frac{\partial^2 \theta}{\partial z^2},\tag{45}$$

where  $\theta(z,t)$  is the volumetric water content at position z and time t,  $D_0$  is the diffusion coefficient of water in the paper, and z is the coordinate across the paper's thickness. Under steady-state conditions, the moisture content does not change with time  $(\partial \theta/\partial t = 0)$ , simplifying the equation to:

$$D_0 \frac{d^2 \theta}{dz^2} = 0. \tag{46}$$

Integrating this equation twice with respect to z yields a linear moisture profile:

$$\theta(z) = az + b, (47)$$

where a and b are constants determined by the boundary conditions. To solve for a and b, we apply the following boundary conditions:

#### 1. Saturation at the Bottom Surface (z=0)

The bottom surface of the paper is in contact with water, so it remains saturated:

$$\theta(0) = \theta_{\text{sat}},\tag{48}$$

where  $\theta_{\rm sat}$  is the saturated volumetric water content. This condition implies:

$$b = \theta_{\text{sat}}. (49)$$

**2.Evaporation at the Top Surface** (z = h) The top surface experiences evaporation, introducing a flux boundary condition based on Fick's First Law:

$$-D_0 \left. \frac{d\theta}{dz} \right|_{z=h} = \frac{q}{A},\tag{50}$$

where q is the volumetric evaporation rate and A is the surface area of the paper. The derivative  $\frac{d\theta}{dz}$  at z=h is equal to a, leading to:

$$-D_0 a = \frac{q}{A} \implies a = -\frac{q}{AD_0}.$$
 (51)

Substituting a and b back into the moisture profile gives:

$$\theta(z) = -\frac{q}{AD_0}z + \theta_{\text{sat}}.$$
 (52)

This linear profile indicates that the moisture content decreases from the saturated value at the bottom to a lower value at the top due to evaporation. The variation in moisture content induces strain within the paper, as different layers swell to different extents. The strain due to moisture content at any position z is proportional to the local moisture content relative to saturation:

$$\epsilon_{\theta}(z) = \epsilon_{\text{sat}} \frac{\theta(z)}{\theta_{\text{sat}}},$$
(53)

where  $\epsilon_{\rm sat}$  is the strain at full saturation.

The total strain in the paper combines the mechanical strain due to bending,  $\epsilon_{\kappa}(z)$ , and the hygroscopic strain due to moisture,  $\epsilon_{\theta}(z)$ :

$$\epsilon(z) = \epsilon_{\kappa}(z) - \epsilon_{\theta}(z). \tag{54}$$

According to beam theory, the mechanical strain from bending is:

$$\epsilon_{\kappa}(z) = -\kappa(z - z_n),\tag{55}$$

where  $\kappa$  is the curvature and  $z_n$  is the position of the neutral axis, assumed to be at the mid-thickness for symmetry.

For mechanical equilibrium, the net strain gradient across the thickness must be zero:

$$\frac{d\epsilon}{dz} = -\kappa - \frac{d\epsilon_{\theta}}{dz} = 0 \implies \kappa = -\frac{d\epsilon_{\theta}}{dz}.$$
 (56)

Differentiating the moisture-induced strain with respect to z yields:

$$\frac{d\epsilon_{\theta}}{dz} = \epsilon_{\text{sat}} \frac{1}{\theta_{\text{sat}}} \frac{d\theta}{dz} = -\epsilon_{\text{sat}} \frac{1}{\theta_{\text{sat}}} \frac{q}{AD_0}.$$
 (57)

Substituting this back into the expression for curvature gives:

$$\kappa = -\left(-\epsilon_{\text{sat}} \frac{1}{\theta_{\text{sat}}} \frac{q}{AD_0}\right) = \epsilon_{\text{sat}} \frac{q}{\theta_{\text{sat}} AD_0}.$$
 (58)

The final expression reveals that the curvature  $\kappa_{\text{final}}$  is directly proportional to the evaporation rate q and the saturated strain  $\epsilon_{\text{sat}}$ , while inversely proportional to the saturated water content  $\theta_{\text{sat}}$ , the surface area A, and the diffusion coefficient  $D_0$ :

$$\kappa_{\text{final}} = \frac{\epsilon_{\text{sat}} q}{\theta_{\text{sat}} A D_0}.$$
 (59)

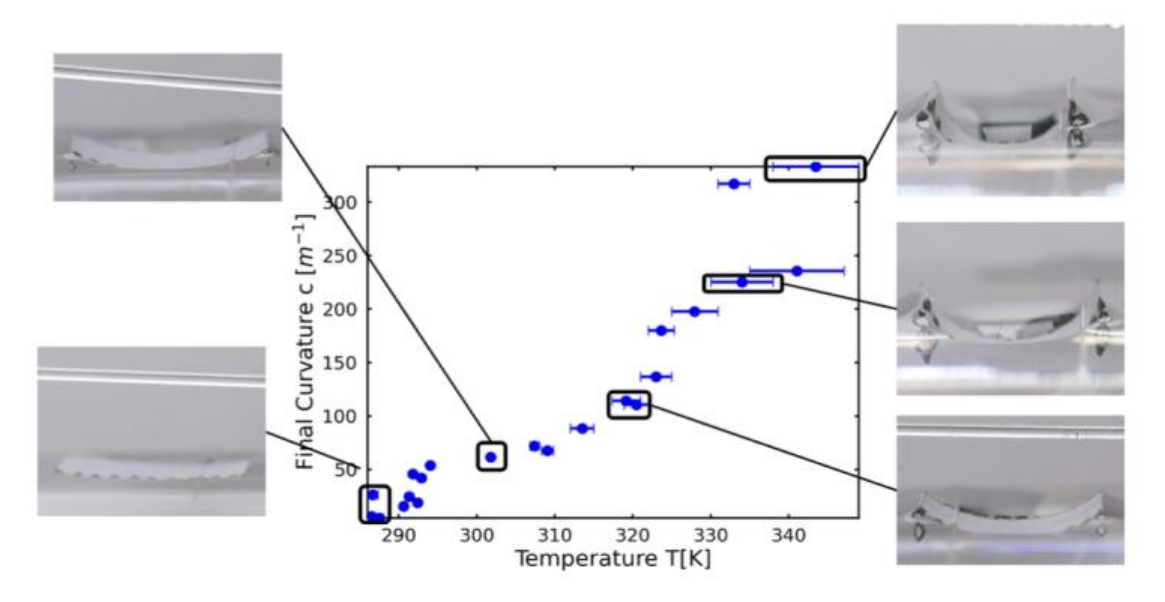


Figure 26: Relationship of final curvature under different temperatures and their corresponding ratio of surface tension and viscosity.

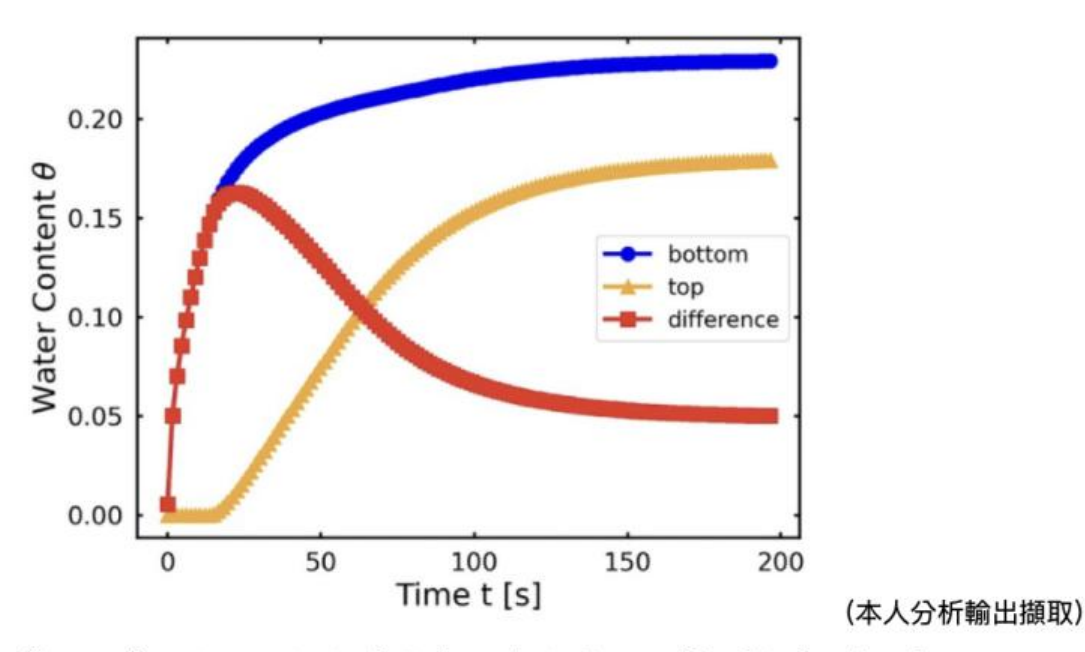


Figure 27: Curve of water content plotted against time. Simulated using  $h=87.15\,\mu\mathrm{m},\,\frac{q}{AD_0}=0.01\,\mu\mathrm{m},\,\theta_\mathrm{sat}=0.25.$  Water content of top and bottom are averages of upper half and lower half part of paper.

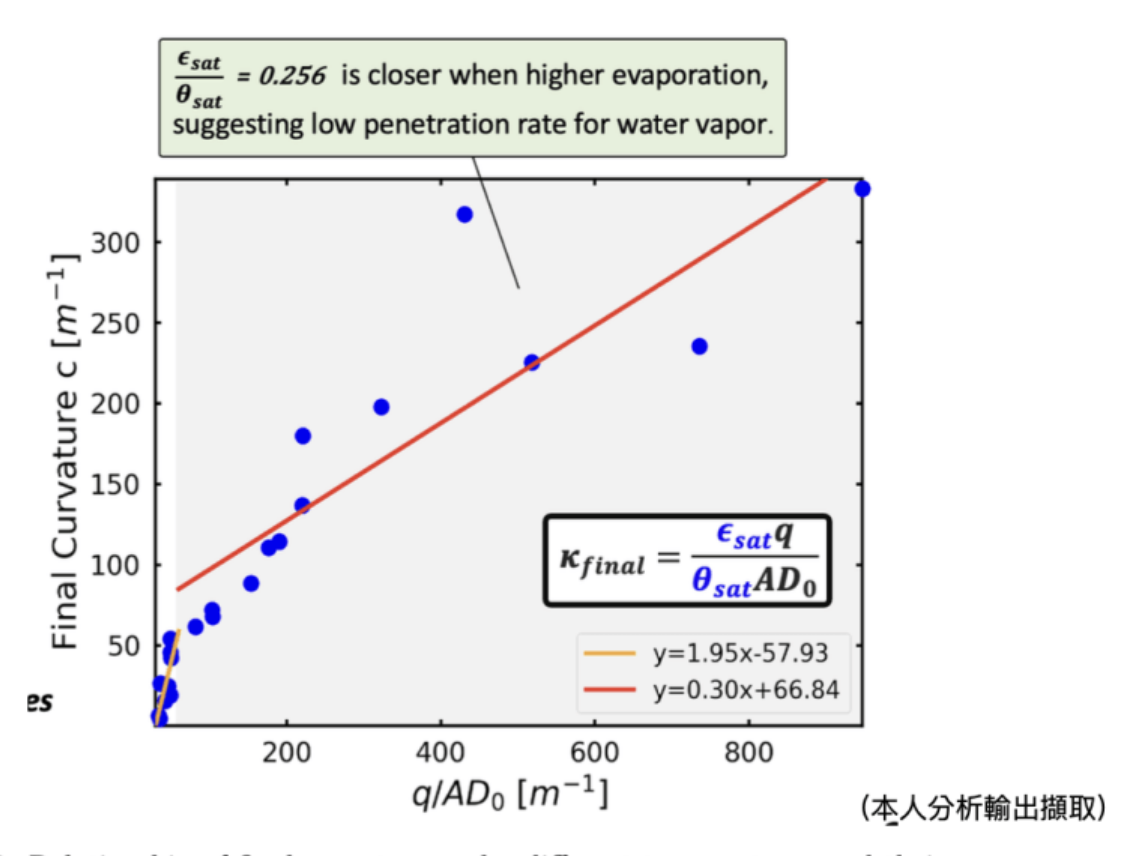


Figure 28: Relationship of final curvature under different temperatures and their corresponding ratio of surface tension and viscosity.

# (VI.)Discussion-Salt Concentration

Salt concentration changes both viscosity and surface tension, and by assuming cylindrical pores, formula (5), we see that the diffusivity is linearly related to the ratio  $\frac{\gamma}{\mu}$ . The experimental data also supports this fact. Further investigations in contact angle may reveal more about the average pore size and pore distribution, and how they can fix the cylindrical pore formula, which is clearly not the case for n = 1.1. It should be noted that the model only predicts the peak curvature is determined by expansion and thickness alone. Nevertheless, increasing salt concentration also increases the peak curvature. This cannot be explained by our theory alone, since salt concentration does not affect the maximum expansion, and thickness is controlled throughout the experiment.

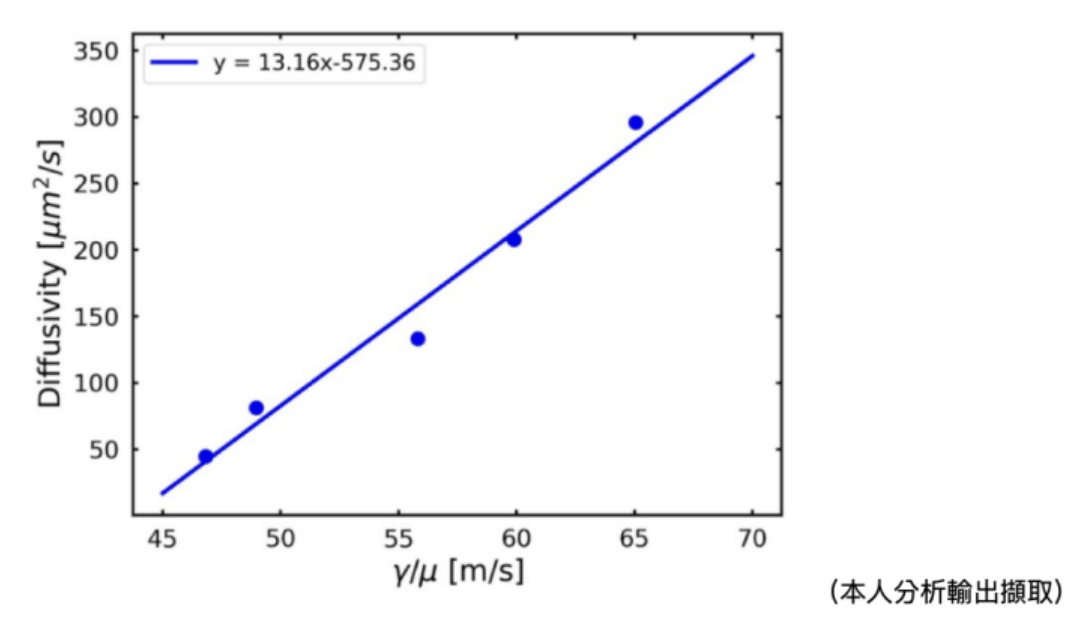


Figure 29: Linear relationship between diffusivity and ratio of surface tension and viscosity. This supports capillary theory, yet the description of slope need further improvements.

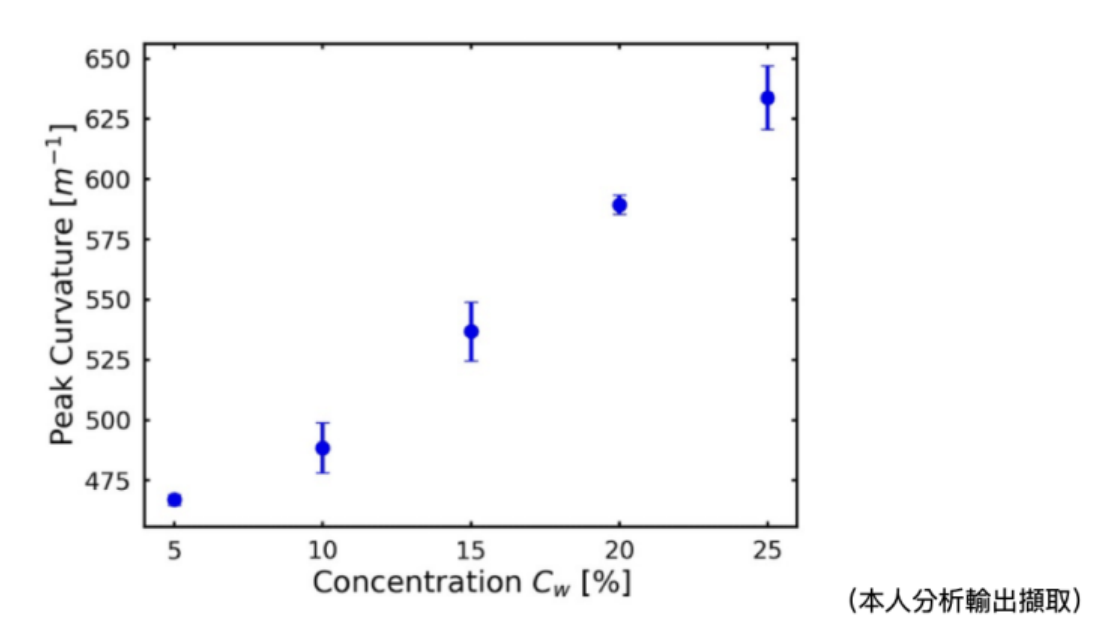


Figure 30: Peak curvature increases with salt concentration. This shows a limitation of the theory, which predicts little change in peak curvature.

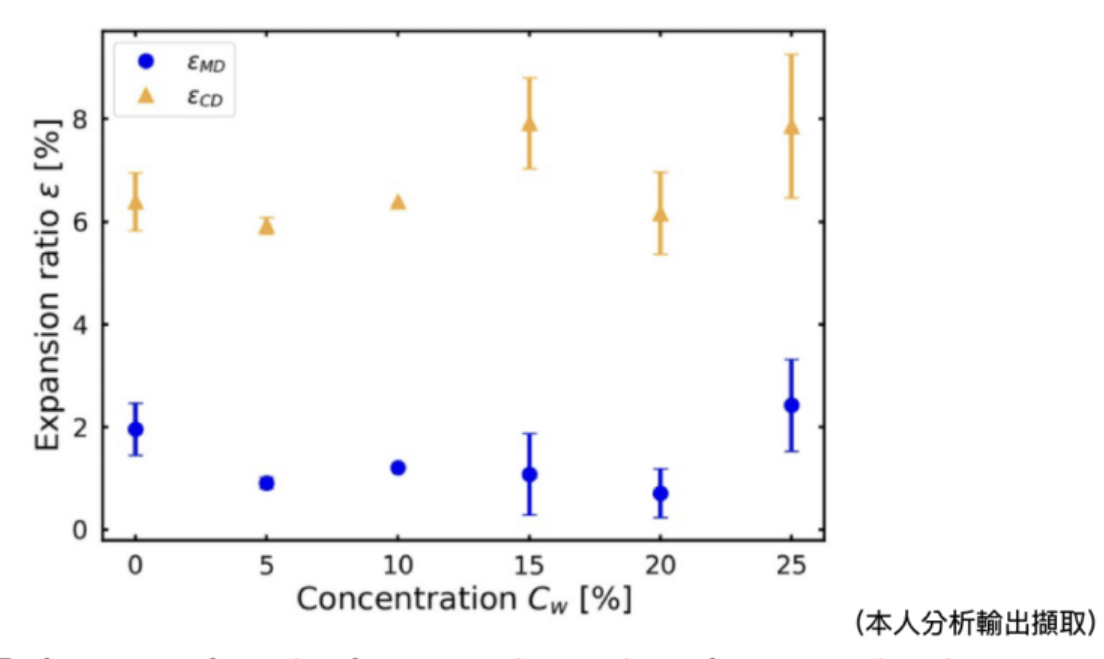
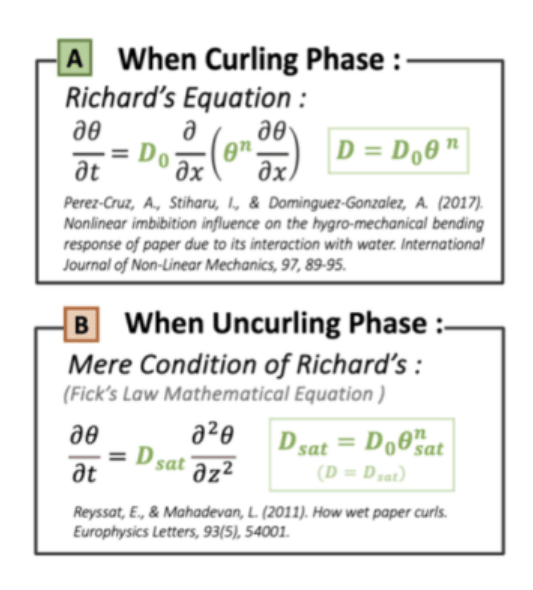
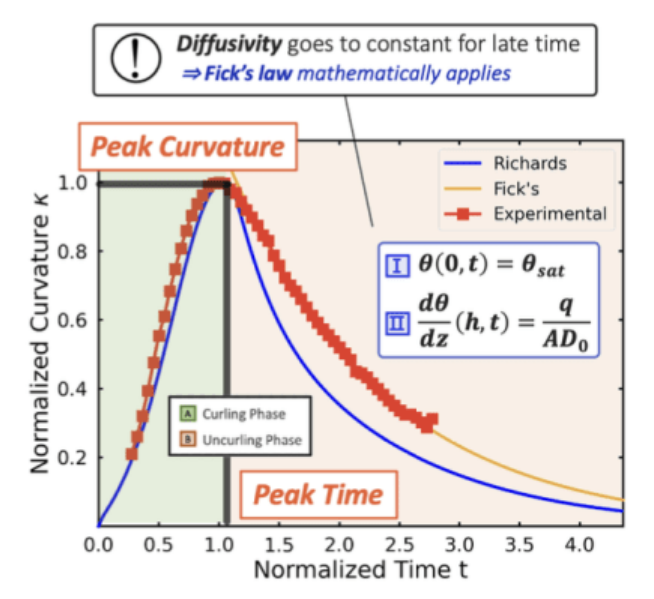


Figure 31: Peak curvature change in salt concentration case is not due to expansion, since saturated expansion rate does not change with salt concentration.

# V. Conclusion

# (I.) Own Mechanism Explanation





(本人繪製、分析輸出擷取)

Our research introduces a new understanding of the curling and uncurling behavior of tracing paper when interacting with water, resolving limitations in prior models based on Fick's second law of diffusion. While Fick's model adequately described the uncurling phase, it failed to accurately capture the curling phase due to significant deviations in the underlying mechanism. Through our investigation, we identified capillary action, more accurately represented by Richard's equation, as the fundamental process governing the curling phenomenon.

During the curling phase, we observed that diffusivity is not constant but changes dynamically in relation to the water content within the paper. This dynamic diffusivity aligns with the capillary-driven nature of water movement through the porous structure of tracing paper. Our experimental results demonstrated a precise fit with the theoretical model based on Richard's equation, confirming that diffusivity reaches a peak as the water content becomes saturated.

As the system transitions to the uncurling phase, the water content remains saturated, and the diffusivity stabilizes to a constant value. Under these conditions, Fick's law becomes mathematically applicable, and the observed exponential decay in curvature aligns with previous literature modeling this phase using diffusion principles.

Our contribution lies in bridging the gap between observed experimental data and the theoretical modeling of the curling phase. By incorporating the capillary mechanism and accounting for the variable diffusivity dependent on water content, we provided a more accurate and comprehensive model, resolving discrepancies found in prior studies and enhancing the fundamental understanding of moisture-induced deformation in porous materials.

At the peak curvature, it is crucial to note that saturated water content does not imply complete pore saturation within the tracing paper. Instead, saturation signifies that water penetration has reached a steady state where no additional water can infiltrate the pores. This steady state is achieved even if some pores remain unfilled, primarily due to water evaporation processes that prevent complete saturation of all available pores.

# (II.) Our Simulation-Finite Difference Approximating Scheme

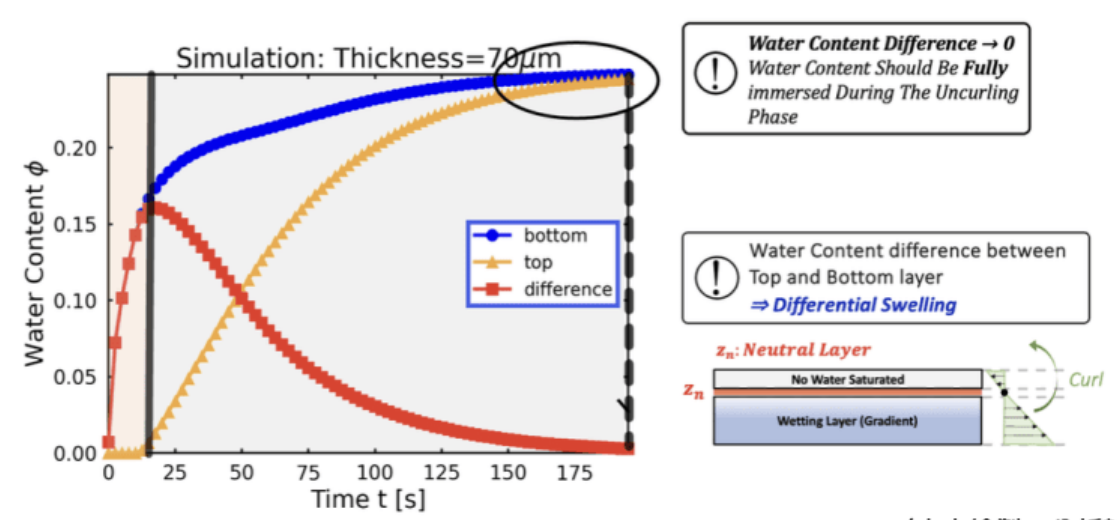
In this work, we have developed a novel finite difference approximation scheme to simulate the wetting and curling of paper, grounded in the Richards equation. By explicitly expanding the Richards equation using the product rule, we set the foundation for a detailed and controllable simulation process without reliance on commercial software. Our approach begins with discretizing the spatial domain into N+1 intervals and N points, each separated by  $\Delta z$ , allowing for precise control over spatial resolution.

For computational simplicity and efficiency, we employed a forward difference scheme.

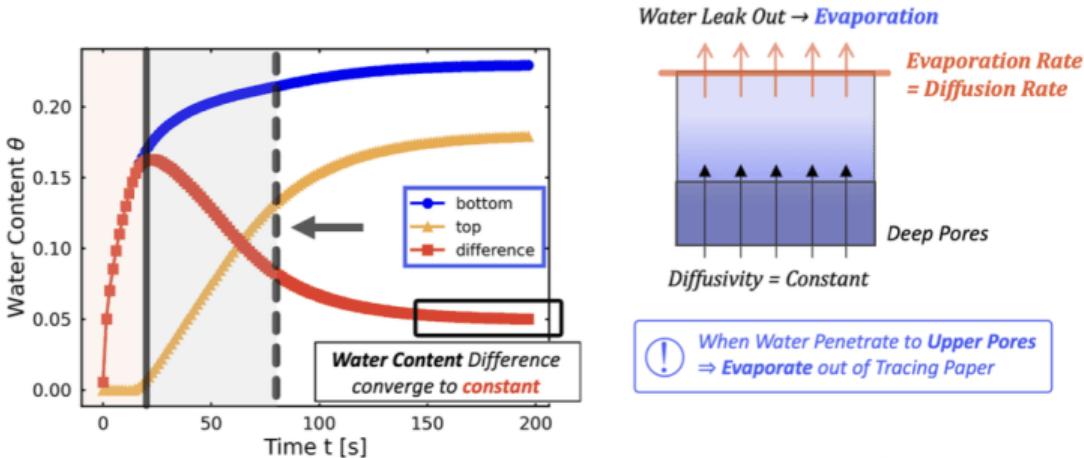
While recognizing that convergence criteria for linear diffusion (as described by Fick's law) may not directly apply to our nonlinear case, we used these criteria as a guiding reference for selecting appropriate time and spatial steps. A significant challenge we addressed was the implementation of the Robin boundary condition. We introduced a column of virtual points to extend the iteration to n = N, enabling the application of central difference approximations for spatial derivatives alongside forward differences for time steps.

An initial obstacle arose due to the imposed initial condition where the paper, except at the water surface, was devoid of water. This led to zero propagation of moisture in the simulation, as the approximation scheme multiplied the current water content, resulting in a static solution over time. To overcome this, we introduced the assumption that the spatial variation of water content is small. This critical insight allowed us to approximate the water content at any given point using adjacent points (or a single point at the boundary), facilitating the propagation of moisture through the paper in the simulation.

Our methodology successfully integrates the Richards equation with tailored boundary and initial conditions to model the complex phenomena of paper wetting and curling. The finite difference approximation scheme we developed is, to the best of our knowledge, unprecedented in existing literature. I wrote them here. I used no commercial software to do the simulation. Thus, this work providing a clear and controlled simulation framework that advances the understanding of moisture dynamics in porous materials like paper.



(本人繪製、分析輸出擷取)



(本人繪製、分析輸出擷取)

Qualitative analysis of water penetration into tracing paper—supported by simulations of Richards' equation—highlights the critical role of evaporation in the curling behavior observed. Initially, when the tracing paper is placed on the water surface, the water content difference between the top and bottom layers increases. This gradient leads to differential swelling, causing the paper to curl rapidly during the initial phase.

By employing simulations of Richards' equation both **with** and **without** the consideration of evaporation, we elucidated the critical role that evaporation plays in accurately modeling moisture dynamics and the resulting mechanical deformation of porous materials.

In the simulation without evaporation, placing the tracing paper on the water surface led to an increasing water content difference between the bottom (in contact with water) and the top layers. This gradient induced differential swelling, causing the paper to curl rapidly—a phase identified as the *curling phase*. Over time, this model predicted that the water content difference would diminish to zero, implying full saturation of the tracing paper and the cessation of curvature changes. However, this outcome did not align with experimental observations, indicating that the model lacked essential factors influencing the actual behavior.

Introducing evaporation into the Richards' equation simulation yielded results that more accurately reflected experimental findings. Initially, the water content difference increased similarly to the non-evaporation model, leading to rapid curling due to differential swelling. After reaching a maximum, the water content difference began to decrease and eventually stabilized at a constant value rather than reducing to zero. This steady state occurred because the evaporation rate from the top layer balanced the diffusion rate of water moving upward through the paper. The continuous

removal of moisture from the top layer was compensated by water diffusing from the wetter bottom layers, maintaining a constant water content difference across the paper's thickness.

At this late stage, Fick's law became applicable due to the establishment of a steady-state moisture gradient. The maintained water content difference resulted in a uniform diffusion flux, satisfying the conditions where Fick's law accurately describes the system's behavior. The tracing paper reached a form of saturated water content—not implying that all pores were fully saturated, but that the moisture distribution had reached equilibrium given the ongoing evaporation. This mechanism explained why the curvature decreased after reaching a maximum and then remained constant; the differential swelling stabilized because the water content difference no longer changed significantly over time.

Our findings underscore the **critical importance of considering evaporation** when modeling the moisture-induced deformation of porous materials like tracing paper. The simulation incorporating evaporation aligned closely with experimental observations and validated the theoretical model of curvature previously discussed.

### (III.) Own Contribution-Key Parameters Discussion

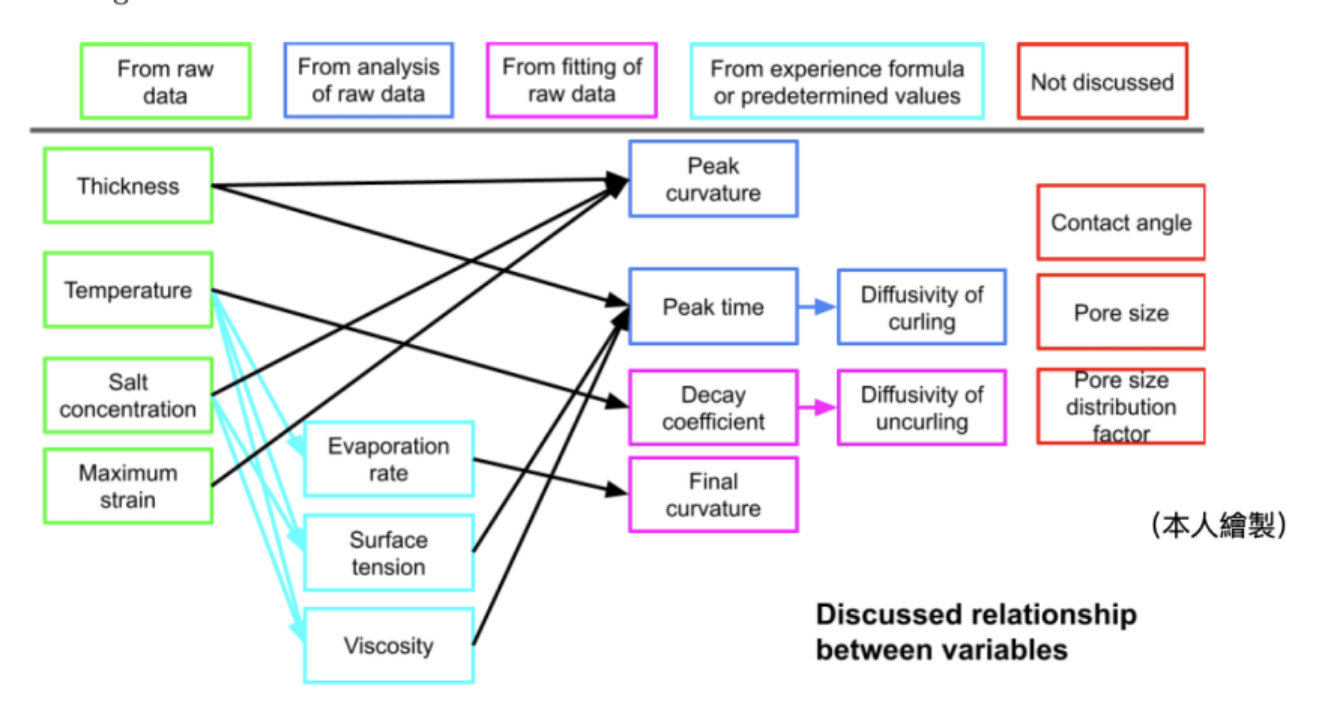
Moreover, our research elucidates how key parameters depend on thickness, temperature, and salt concentration in the wetting-induced curling behavior of tracing paper. The geometry of curling—including the curling direction, the number of cylinders formed, and whether the paper sinks—is influenced by factors such as anisotropy of expansion, release angle, and the dimensions of the paper. We established a linear relationship between peak time and the reciprocal of thickness, as well as between peak curvature and the square of thickness, confirming theoretical predictions.

In exploring temperature dependence, an area not previously examined, we discovered that varying temperature affects both viscosity and surface tension, thereby influencing the diffusivity of water into the paper. Temperature also impacts peak curvature and curling speed, both of which increase as the paper softens with rising temperatures. At higher temperatures, the paper does not fully uncurl after reaching peak curvature due to evaporation effects, leading to a non-zero final curvature. This underscores the significant role of evaporation in the long-term behavior of curling, which previous studies have not considered.

Regarding salt concentration, our experiments yielded unexpected results. While surfactant molecules cannot penetrate the cellulose surface and were anticipated to have minimal effect, increasing salt concentration led to a rise in peak curvature even though the expansion ratio remained unchanged. This suggests that factors beyond thickness

and maximum strain influence peak curvature, indicating the need for theoretical amendments.

By establishing linear relationships and identifying previously unconsidered factors like evaporation, we contribute significant insights to the understanding of fluid dynamics in thin porous materials, enhancing theoretical models and opening avenues for future investigation.



## VI.References

- Klemm, D., Philipp, B., Heinze, T., Heinze, U., & Wagenknecht, W. (1998). Comprehensive cellulose chemistry: Volume 1: Fundamentals and analytical methods.
   Wiley-VCH Verlag GmbH. ISBN:978-3-527-60192-9
- [2] Kjellgren, H. (2007). Influence of paper properties and polymer coatings on barrier properties of greaseproof paper (Doctoral dissertation, Karlstad University Studies, 2007:40). Karlstad University. ISBN:978-91-7063-144-3
- [3] Huinink, Henk, Philip Ruijten, and Thomas Arends. (2016). Fluids in Porous Media: Transport and Phase Changes. San Rafael, CA: Morgan Claypool Publishers.

- [4] Nissan, A. H. (1976). H-Bond Dissociation in Hydrogen Bond Dominated Solids. *Macromolecules*, 9(5), 840–850. https://doi.org/10.1021/ma60053a026.
- [5] Penfold, J., Tucker, I., Petkov, J., & Thomas, R. K. (2007). Surfactant Adsorption onto Cellulose Surfaces. *Langmuir*, 23(16), 8357–8364. https://doi.org/10.1021/la700948k.
- [6] Perez-Cruz, Angel, Ion Stiharu, and Aurelio Dominguez-Gonzalez. (2017a). Non-linear Imbibition Influence on the Hygro-Mechanical Bending Response of Paper Due to Its Interaction with Water. *International Journal of Non-Linear Mechanics*, 97(December), 89–95. https://doi.org/10.1016/j.ijnonlinmec.2017.09.002.
- [7] Perez-Cruz, Angel, Ion Stiharu, and Aurelio Dominguez-Gonzalez. (2017b). Two-Dimensional Model of Imbibition into Paper-Based Networks Using Richards' Equation. *Microfluidics and Nanofluidics*, 21(5), 98. https://doi.org/10.1007/s10404-017-1937-0.
- [8] Reyssat, E., & Mahadevan, L. (2011). How Wet Paper Curls. *EPL (Europhysics Letters)*, 93(5), 54001. https://doi.org/10.1209/0295-5075/93/54001.
- [9] Swedish Forest Products Research Laboratory, Stockholm, A. De Ruvo, R. Lundberg, S. Martin-Löf, and C. Söremark. (1973). Influence of Temperature and Humidity on the Elastic and Expansional Properties of Paper and the Constituent Fibre. In F. Bolam (Ed.), Trans. of the Vth Fund. Res. Symp. Cambridge, 1973 (pp. 785–806). Fundamental Research Committee (FRC), Manchester. https://doi.org/10.15376/frc.1973.2.785.
- [10] 中華民國地 64 中小學科學展覽會高雄市科展作品:描圖紙沾溼捲曲行為機制探討

# Appendix 1: Simulation Code

The following pseudocode was used to simulate the Richards' prediction with Dirichlet and Robin boundary conditions:

```
dx = 0.9
x_real = np.arange(0, length + dx, dx)
x_vec = np.arange(0, len(x_real))

dt = 0.001
t_real = np.arange(0, total_time + dt, dt)
t_vec = np.arange(0, len(t_real) - 1) # Richards' Prediction
u[:, 0] = phi_sat
```

```
for t in t_vec:
    for x in x_vec:
        if x == x_{vec}[0]:
            continue
        if x == x_{vec}[-1]:
            u[t+1, x] = u[t, x] + r*D0*(u[t, x-1])**m *
                        (2*u[t, x-1] + u[t, x] * (m*c**2*dx**2 - 2*c*dx - 2))
            continue
        u[t+1, x] = u[t, x] + r*D0*((u[t, x-1] + u[t, x+1])/2)**(m-1) *
                    ((m/4)*(u[t, x+1] - u[t, x-1])**2 +
                    u[t, x]*(u[t, x+1] + u[t, x-1]) - 2*u[t, x]**2)
# Dirichlet Boundary, Robin(n=N) Boundary, Normal iteration
r = dt / dx^2
c = 0.01
u = np.zeros([len(t_real), len(x_real)]) # Visualization
phi_richards = u
for t in t_vec:
    phi_richards_bottom[t] = np.average(phi_richards[t, :len(x_real)//2])
    phi_richards_top[t] = np.average(phi_richards[t, len(x_real)//2+1:])
```

# Appendix 2: Finite Difference Approximation for Fick's Second Law

Applying the finite difference method to Eq.(14), we discretize the time and space domains similarly as before. The time derivative is approximated using a forward difference:

$$\left. \frac{\partial \theta}{\partial t} \right|_{n}^{k} \approx \frac{\theta_{n}^{k+1} - \theta_{n}^{k}}{\Delta t},$$
 (60)

and the second spatial derivative is approximated using a central difference:

$$\left. \frac{\partial^2 \theta}{\partial z^2} \right|_n^k \approx \frac{\theta_{n+1}^k - 2\theta_n^k + \theta_{n-1}^k}{\Delta z^2}. \tag{61}$$

Substituting these approximations into Eq.(14), we obtain the update formula for each interior node  $(1 \le n \le N - 1)$ :

$$\theta_n^{k+1} = \theta_n^k + \frac{D\Delta t}{\Delta z^2} \left( \theta_{n+1}^k - 2\theta_n^k + \theta_{n-1}^k \right). \tag{62}$$

The boundary conditions remain the same as in the Richards' equation simulation. At n = 0, we apply the Dirichlet boundary condition:

$$\theta_0^k = \theta_{\text{sat}},\tag{63}$$

and at n = N, we implement the Robin boundary condition to model evaporation:

$$\left. \frac{\partial \theta}{\partial z} \right|_{z=b} = -c\theta_N^k. \tag{64}$$

Discretizing the Robin boundary condition using a backward difference for the derivative yields:

$$\frac{\theta_N^k - \theta_{N-1}^k}{\Delta z} = -c\theta_N^k,\tag{65}$$

which can be rearranged to solve for  $\theta_{N-1}^k$ :

$$\theta_{N-1}^k = \theta_N^k \left( 1 + c\Delta z \right). \tag{66}$$

Substituting this into the update formula for n = N:

$$\theta_N^{k+1} = \theta_N^k + \frac{D\Delta t}{\Delta z^2} \left( \theta_{N+1}^k - 2\theta_N^k + \theta_{N-1}^k \right).$$
 (67)

Since  $\theta_{N+1}^k$  is beyond our domain, we can assume that the flux at n = N + 1 is governed by the boundary condition, or we can adjust the finite difference stencil at the boundary to use a one-sided difference.

Listing 1: Fick's Law Prediction

# Fick's prediction
r = dt / dx\*\*2
C = 0.01
u[:, 0] = phi\_sat # u(t, 0) = 0.25

for t in t\_vec:

```
for x in x_vec:
        if x == x_vec[0]:
             continue
        if x == x_vec[-1]:
             u[t+1, x] = D0 * (
                 2 * r * u[t, x-1] - 2 * r * u[t, x]
                 - 2 * r * C * dx * u[t, x]
             ) + u[t, x]
             continue
        u[t+1, x] = D0 * (
             r * u[t, x+1] - 2 * r * u[t, x] + r * u[t, x-1]
        ) + u[t, x]
phi_ficks = u
for t in t_vec:
    phi_ficks_bottom[t] = np.average(
        phi_ficks[t, :len(x_real)//2]
    phi_ficks_top[t] = np.average(
        phi_ficks[t, len(x_real)//2+1:]
    )
             0.25
            0.20
         Water Content \phi
             0.15
                                                        top
                                                        difference
             0.10
             0.05
             0.00
                                   50
                                            75
                           25
                                                   100
                                   Time [s]
```

Figure 32: Fick's Simulation of water content-without evaporation

(本人分析輸出擷取)

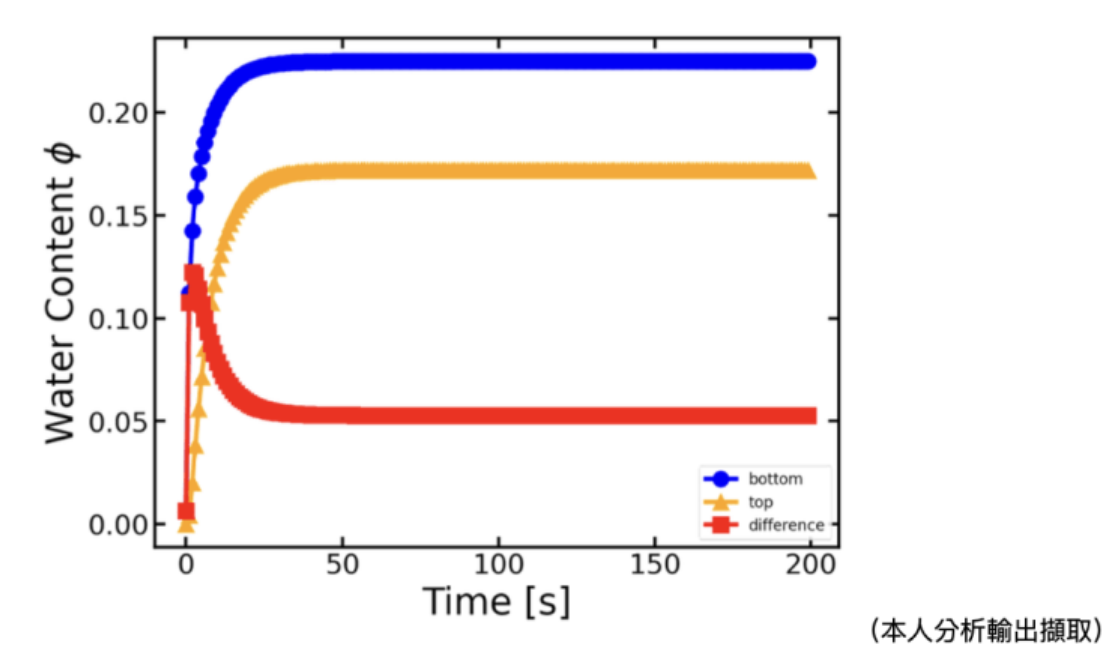


Figure 33: Fick's Simulation of water content

#### Alternate Approach Using Fick's Second Law

As an alternative to Richards' equation, we consider modeling the moisture diffusion in paper using Fick's second law of diffusion. Fick's second law in one dimension is expressed as:

$$\frac{\partial \theta}{\partial t} = D \frac{\partial^2 \theta}{\partial z^2},\tag{68}$$

where  $\theta(z,t)$  represents the moisture content (analogous to concentration), and D is the constant diffusion coefficient.

### Finite Difference Approximation for Fick's Second Law

Applying the finite difference method to Eq. (68), we discretize the time and space domains similarly as before. For the explicit finite difference scheme applied to Fick's second law, the stability criterion is well-known and given by:

$$\frac{D\Delta t}{\Delta z^2} = Dr \le \frac{1}{2}. (69)$$

This criterion guides the selection of  $\Delta t$  and  $\Delta z$  to ensure stable and accurate simulations. The time derivative is approximated using a forward difference:

$$\left. \frac{\partial \theta}{\partial t} \right|_{n}^{k} \approx \frac{\theta_{n}^{k+1} - \theta_{n}^{k}}{\Delta t},$$
 (70)

and the second spatial derivative is approximated using a central difference:

$$\left. \frac{\partial^2 \theta}{\partial z^2} \right|_n^k \approx \frac{\theta_{n+1}^k - 2\theta_n^k + \theta_{n-1}^k}{\Delta z^2}. \tag{71}$$

Substituting these approximations into Eq. (68), we obtain the update formula for each interior node  $(1 \le n \le N - 1)$ :

$$\theta_n^{k+1} = \theta_n^k + \frac{D\Delta t}{\Delta z^2} \left( \theta_{n+1}^k - 2\theta_n^k + \theta_{n-1}^k \right). \tag{72}$$

Defining the diffusion number r as:

$$r = \frac{\Delta t}{\Delta z^2},\tag{73}$$

we can rewrite the update formula as:

$$\theta_n^{k+1} = \theta_n^k + Dr \left( \theta_{n+1}^k - 2\theta_n^k + \theta_{n-1}^k \right). \tag{74}$$

### **Boundary and Initial Conditions**

The boundary conditions remain the same as in the Richards' equation simulation. At n = 0, we apply the Dirichlet boundary condition:

$$\theta_0^k = \theta_{\text{sat}},\tag{75}$$

and at n = N, we implement the Robin boundary condition to model evaporation:

$$\left. \frac{\partial \theta}{\partial z} \right|_{z=h} = -c\theta_N^k,\tag{76}$$

where c is the evaporation coefficient.

Discretizing the Robin boundary condition using a backward difference yields:

$$\frac{\theta_N^k - \theta_{N-1}^k}{\Delta z} = -c\theta_N^k,\tag{77}$$

which rearranges to:

$$\theta_{N-1}^k = \theta_N^k (1 + c\Delta z). \tag{78}$$

Substituting Eq. (78) into the update formula for n = N:

$$\theta_N^{k+1} = \theta_N^k + Dr\left(\theta_{N+1}^k - 2\theta_N^k + \theta_N^k (1 + c\Delta z)\right). \tag{79}$$

Since  $\theta_{N+1}^k$  lies outside our domain, we can assume  $\theta_{N+1}^k = \theta_N^k$  (assuming zero flux beyond the boundary). Thus, Eq. (79) simplifies to:

$$\theta_N^{k+1} = \theta_N^k + Dr\left(\theta_N^k - 2\theta_N^k + \theta_N^k (1 + c\Delta z)\right) \tag{80}$$

$$= \theta_N^k + Dr\left(c\Delta z \theta_N^k\right). \tag{81}$$

Alternatively, from our code implementation, the update formula at n = N is given by:

$$\theta_N^{k+1} = D\left(2r\theta_{N-1}^k - 2r\theta_N^k - 2rc\Delta z\theta_N^k\right) + \theta_N^k. \tag{82}$$

Substituting  $\theta_{N-1}^k = \theta_N^k (1 + c\Delta z)$  into Eq. (82):

$$\theta_N^{k+1} = D \left[ 2r\theta_N^k (1 + c\Delta z) - 2r\theta_N^k - 2rc\Delta z\theta_N^k \right] + \theta_N^k \tag{83}$$

$$=\theta_N^k. \tag{84}$$

This indicates that the net change at n = N is zero, suggesting that the moisture content remains constant at the boundary node when using this approximation. Comparing Eqs. (81) and (82), we observe that both formulations aim to incorporate the Robin boundary condition into the finite difference scheme, although they arrive at different conclusions due to the assumptions made about  $\theta_{N+1}^k$ . To reconcile these, we can adjust the finite difference scheme to account for the boundary condition more accurately. By using a one-sided difference at the boundary or modifying the assumption about  $\theta_{N+1}^k$ , we can ensure consistency between the equations.

### Numerical Implementation

The algorithm proceeds as follows:

- 1. Initialize the moisture content at t=0 with  $\theta_n^0=0$  for  $n\geq 1$  and  $\theta_0^0=\theta_{\rm sat}$ .
- 2. For each time step k:
  - (a) For n = 0 (Dirichlet boundary), set  $\theta_0^{k+1} = \theta_{\text{sat}}$ .
  - (b) For n = N (Robin boundary), update  $\theta_N^{k+1}$  using Eq. (81).
  - (c) For interior nodes  $(1 \le n \le N-1)$ , update  $\theta_n^{k+1}$  using Eq. (74).

### **Averaging Moisture Content**

To analyze the moisture distribution and its impact on paper curling, we calculate the average moisture content in the bottom and top halves of the paper:

$$\phi_{\text{bottom}}^k = \frac{2}{N} \sum_{n=0}^{N/2} \theta_n^k, \tag{85}$$

$$\phi_{\text{top}}^k = \frac{2}{N} \sum_{n=N/2+1}^N \theta_n^k. \tag{86}$$

These averages provide insight into the moisture gradients that drive the curling behavior of the paper.

By applying the finite difference method to Fick's second law, we model the moisture diffusion in paper under the assumption of constant diffusivity. This approach simplifies the computational process and allows for direct implementation of standard finite difference schemes without the complexities introduced by the nonlinear terms in Richards' equation. Our method provides an alternative framework for simulating paper wetting, especially when the moisture transport can be approximated as linear diffusion.

# 【評語】160012

這個工作想要找出一個更精確的理論來瞭解在水中紙張的卷曲現象。它提出毛細作用會使水在紙張中的擴散隨水分含量而變化。理論工作相當紮實且深入。報告也寫得很詳盡。建議加入一些討論可以應用此方法的其他研究題材。